2014-07-01

Investigation of a New Method of Estimating Acoustic Intensity and Its Application to Rocket Noise

Benjamin Young Christensen
Brigham Young University - Provo

Investigation of a New Method of Estimating Acoustic Intensity and Its Application to Rocket Noise

Benjamin Young Christensen

A thesis submitted to the faculty of
Brigham Young University
in partial fulfillment of the requirements for the degree of

Master of Science

Kent Gee, Chair
Derek Thomas
Tracianne Neilsen

Department of Physics and Astronomy

Brigham Young University

July 2014

ABSTRACT

Investigation of a New Method of Estimating Acoustic Intensity
and Its Application to Rocket Noise

Benjamin Young Christensen
Department of Physics and Astronomy, BYU
Master of Science

An alternative pressure-sensor based method for estimating the acoustic intensity, the phase and amplitude gradient estimation (PAGE) method, is presented. This method is similar to the finite-difference p-p (FD) method, in which the intensity is estimated from pressure measurements made using an array of closely spaced microphones. The PAGE method uses the same hardware as the FD method, but does not suffer from the frequency-dependent bias inherent to the FD method. Detailed derivations of the new method and the traditional FD method are presented. Both methods are then compared using two acoustic fields: a plane wave and a three monopole system. The ability to unwrap the phase component of the PAGE method is discussed, which leads to accurate intensity estimates above previous frequency limits. The uncertainties associated with both methods of estimation are presented. It is shown that the PAGE method provides more accurate intensity estimates over a larger frequency bandwidth. The possibility of using a higher-order least-squares estimation with both methods is briefly demonstrated. A laboratory experiment designed to validate the PAGE method was conducted. The preliminary results from this experiment are presented and compared to analytical predictions. Finally, the application of the PAGE method to a static rocket test firing is presented. The PAGE method is shown to provide accurate intensity estimates at frequencies that are higher than possible with just the FD method.

Keywords: acoustic intensity, finite-difference, rocket noise

Contents

Chapter 1

Introduction

Almost 100 new satellites are sent into space every year. One concern faced when launching a satellite into space is the protection of sensitive equipment against harmful rocket noise. The noise generated by rockets, or launch vehicles, causes large vibrations that have damaging effects on the launch facilities, the rockets themselves, and their payloads. To be able to protect against and control these vibrations, a better understanding of the generation and propagation of rocket noise is needed.

The models used to predict rocket noise fields are currently validated with far-field pressure measurements.[1] We propose that better validation measurements can be obtained by using near-field, energy-based measurements. These measurements will also provide insight into the physical processes that govern rocket noise generation and propagation. An acoustic, energy-based measurement refers to any measurement of acoustic intensity, sound power, and energy densities. Energy-based quantities are useful in the analysis of rocket noise because they provide more information about source characteristics than simple pressure measurements. Of the various energy-based quantities, this work focusses on acoustic intensity, a vector quantity indicating energy flux, or the sound power per unit area.[2] Assuming small amplitudes and no mean flow, the complex instantaneous intensity in the frequency domain is given by $I = p\mathbf{u}^*$, where p is the complex scalar

measure of pressure and $\mathbf{u}^*$ is the complex conjugate of the particle velocity, a vector. This study is primarily focused on the real part of the complex intensity, known as the active intensity. Because it is a vector, acoustic intensity is often used to localize sound sources.[19] Furthermore, if intensity measurements are made over a closed surface around a source, the acoustic power of that source can be determined.[3] Overall, intensity is preferred over pressure because it provides more information per measurement point.

Researchers at BYU have led the development of new acoustic intensity probes to measure near-field energy quantities in rocket noise.[4–7] Multi-microphone probes are used to estimate pressure gradients, which are then used to calculate acoustic intensity.[8] Traditionally, these gradients have been estimated through a method that involves using the differences of pressures to create a least-squares estimate of particle velocity, which is then used to calculate intensity. This method is known as the p-p method of estimating acoustic intensity, which we will refer to as the FD method.[9]

A new method has been proposed that separates the pressure gradient into phase and amplitude components.[10] The phase gradient is found through a least-squares estimation using pairwise transfer functions between microphones. The amplitude gradient is found through a least-squares method using the magnitude of the complex pressures. This method is called the phase and amplitude gradient estimator (PAGE) method. The analysis and implementation of this new method is the primary focus of this work.

It is found that the new method is superior to the traditional FD method. Where the FD method has a known issue of underestimating the intensity field as frequency increases, the PAGE method does not suffer from this same frequency-dependent bias. Additionally, one of the primary advantages of the new method is that the argument of the transfer functions can be unwrapped. In certain fields, this allows for accurate intensity estimates at frequencies higher than limitations due to the spatial Nyquist limit.

This thesis is laid out in the following manner. First, details of the formulations of the FD and PAGE methods of estimating acoustic intensity are presented in Chapter 2. This chapter comes from a paper submitted to the Journal of the Acoustical Society of America. Phase unwrapping and its limitations are also included in this chapter, as well as special considerations for ensemble averaging. Several comparison cases are included that show how the PAGE method gives superior results in multiple cases. Finally, the chapter ends with an uncertainty analysis, where the effects of calibration error on both methods are presented. A paper written as a part of a Utah NASA Space Grant is included as Chapter 3, which describes recent work to experimentally validate the PAGE method in a laboratory setting. The final chapter outlines an application of the PAGE method to rocket noise and demonstrates how this new method can be used to achieve more accurate intensity measurements of rocket noise.

Chapter 2

A comparison of acoustic intensity estimation techniques

2.1 Introduction

The method for in-air acoustic intensity measurements using matched microphone sets has been sufficiently refined so that it is the subject of several standards.[11,12] Additional standards have been developed for various applications of intensity measurements, including in situ emission pressure level measurements,[13] sound power measurements,[14,15] and determination of sound insulation properties in building acoustics.[16–18] The principles and applications of acoustic intensity are described in a textbook by Fahy[19] and in other handbooks, such as Refs.20–22. These standards and books deal almost exclusively with a method for estimating acoustic intensity that is commonly referred to as the finite-difference p-p method. This method uses multiple matched microphones to estimate the pressure gradient across the microphones, which corresponds to the particle velocity and thereby the acoustic intensity. This method suffers from a frequency-dependent bias: the method underestimates the intensity as frequency approaches the spatial Nyquist frequency, where

half the wavelength of the incoming waves equals the separation distance between microphones within the probe.[23] For the convenience of this work, the finite-difference p-p method is referred to simply as the FD method.

In addition to the FD or p-p method, there are intensity probes based directly on simultaneous pressure and particle velocity measurements, i.e, the p-u method. A commercially available probe uses a pair of heated wires to measure acoustic velocity directly.[24] In environments where significant non-acoustic temperature and velocity fluctuations occur, use of the p-p method has been shown to be more robust[7,21] Recent efforts to develop and use p-p based probes in the near field of rocket and military jet aircraft plumes[4,5,25,26] have served as motivation to examine errors associated with the FD method.

Various studies have investigated how to quantify and reduce errors related to FD processing of p-p probes. These include low-frequency phase mismatch,[27] high-frequency probe performance[28] and the effect of scattering bias,[29,30] as well as the design of multidimensional probes.[31–34] In recent papers, Wiederhold *et al.*[35,36] reviewed many probe designs and considered different schemes for optimal estimation of sound intensity using the FD method. The foundation for all of these studies is the original FD method, which involves sums and differences of complex pressures or cross spectra.

In this work, we propose a new approach for the calculation of acoustic intensity from measured fields, inspired by the work of Mann *et al.*[37] and Mann and Tichy.[2,38] In these works, it is demonstrated that the active and reactive intensities can be written as

$$\mathbf{I}_a = \frac{1}{\omega\rho_0} P^2 \nabla\phi, \tag{2.1a}$$

$$\mathbf{I}_r = -\frac{1}{\omega\rho_0} P \nabla P. \tag{2.1b}$$

These equations are used to investigate the physical meaning of energy-related quantities. When Mann *et al.* compared theoretical results to measured intensities, intensity relations given in

Eqs. (2.1a) and (2.1b) were not used in measurement, but instead the traditional FD method was used.[38] We propose that the expressions given by Mann *et al*. can be used to create a new method of estimating acoustic intensity. The expressions Eqs. (2.1a) and (2.1b) were proposed primarily as theoretical tools, whereas the focus of this work will be the application of these expressions to estimate intensity from physical measurements.

The FD method uses a gradient of the complex pressure to determine acoustic intensity. Rather than estimating the pressure gradient from the complex pressures, the gradients of the pressure phase and amplitude can be estimated separately. Using these gradients, along with a center pressure amplitude, the relations in Eqs. (2.1a) and (2.1b) can be used to estimate the acoustic intensity. We refer to this method as the phase and amplitude gradient estimation method, or the PAGE method.

This chapter develops the mathematical theory of the PAGE method and demonstrates the advantages of this method over the standard FD method. The derivation of the estimation techniques required for both the FD and PAGE methods is given. One primary advantage of the PAGE method over the FD method is that the measured phase differences can be unwrapped, which allows for accurate intensity estimates past the spatial Nyquist limit. A consideration for ensemble averaging is also included, as it differs slightly between the two methods. We then compare the two methods through estimation error of various fields, using two simple probe configurations. It is shown that the PAGE method does not suffer from the frequency-dependent bias and provides better estimates of the intensity. Lastly, the effects of calibration errors on measurements are considered using an uncertainty analysis.

2.2 Theory

All the derivations in this chapter are conducted in the frequency domain; that is, all pressures and particle velocities are assumed to be obtained from the Fourier transform of an appropriate function. Variables with numeric subscripts correspond to those evaluated at position vectors with the same index. For example, p_1 is equivalent to $p(\mathbf{r}_1)$, where $\mathbf{r}_1$ is a position vector. The methods presented here assume that the measured field is statistically stationary and ergodic, meaning the statistical properties can be determined with a sufficiently long sample.[29] This assumption allows the development of concise frequency-dependent expressions for the complex intensity in terms of active, $\mathbf{I}_a$, and reactive, $\mathbf{I}_r$, components.

Because both the standard FD method and the new PAGE method for estimating the acoustic intensity can be formulated in terms of least-squares estimates, we first present the formulation of this least-squares estimate. The formulation given here provides the same expressions for the estimated pressure gradient as the method of Pascal and Li.[39] However, the approach developed here is better suited to estimation of the gradient of other field quantities required for this work.

2.2.1 Least-squares estimate of the gradient of a scalar function

A probe consisting of N sensors placed at N unique points with position vectors $\mathbf{r}_1, \mathbf{r}_2, \cdots, \mathbf{r}_N$ can be used to estimate the gradient of a scalar function $g(\mathbf{r})$. It should be noted the methods presented here require at least one more sensor than the number of dimensions in the system that is to be measured (i.e. two sensors for one-dimensional fields, three sensors for two-dimensional fields, etc.). The estimate is developed in a geometry-independent form by defining the $N(N-1)/2 \times 3$ matrix $\mathbf{X}$ with unique pairwise separation vectors as rows:

$$\mathbf{X} = [\mathbf{r}_2 - \mathbf{r}_1 | \mathbf{r}_3 - \mathbf{r}_1 | \cdots | \mathbf{r}_N - \mathbf{r}_{N-1}]^T \tag{2.2}$$

and the $1 \times N(N-1)/2$ vector of unique pairwise differences of the values of the function g at the sensor positions:

$$\mathbf{\Delta}g = \begin{bmatrix} g(\mathbf{r}_2) - g(\mathbf{r}_1) \\ g(\mathbf{r}_3) - g(\mathbf{r}_1) \\ \vdots \\ g(\mathbf{r}_N) - g(\mathbf{r}_{N-1}) \end{bmatrix}. \tag{2.3}$$

The gradient of $g(\mathbf{r})$ can be estimated from the approximate relationship:

$$\mathbf{X}\nabla g = \mathbf{\Delta}g + O\left\{\max\left[\mathbf{X}\nabla(\nabla g)\mathbf{X}^T\right]\right\}, \tag{2.4}$$

where $\nabla(\nabla g)$ is the matrix of second-order derivatives of the function g (the Hessian matrix). The order of the error in Eq. (2.4) is approximately proportional to the product of the maximum second derivative and the square of the maximum separation distance between sensors. Because the Hessian matrix can be related to the curvature of isosurfaces in the field g, Eq. (2.4) implies that the local maximum "radius of curvature" of the field g must be large relative to the square of the maximum separation distance of the sensors in the probe. In other words, the field must be close to planar in the neighborhood of the probe.

For probe configurations in which the product of the squared maximum separation distance with the maximum second derivative is sufficiently small compared to the function value, a first-order estimate is obtained from the least-squares solution for the over-determined system in Eq. (2.4):

$$\widehat{\nabla g} = \left(\mathbf{X}^T\mathbf{X}\right)^{-1}\mathbf{X}^T\mathbf{\Delta}g. \tag{2.5}$$

The overhat is used to indicate estimated quantities. The matrix inversion in Eq. (2.5) requires that $\det\left(\mathbf{X}^T\mathbf{X}\right) \neq 0$. A necessary and sufficient condition to be able to invert the matrix $\mathbf{X}^T\mathbf{X}$ for a two-dimensional probe is that the sensors not lie on a line; for a three-dimensional probe, the sensors cannot lie in a plane.

2.2.2 Finite-difference p-p (FD) method

The finite-difference p-p (FD) method relies on a least-squares estimate of the gradient of the complex pressure. The FD estimate of the gradient of a pressure field p is given by Eq. (2.5) as

$$\widehat{\nabla p} = \left(\mathbf{X}^T\mathbf{X}\right)^{-1}\mathbf{X}^T\mathbf{\Delta}p. \tag{2.6}$$

The expression for the estimated pressure gradient $\widehat{\nabla p}$ in Eq. (2.6) is a linear combination of the pressures measured at the sensor locations. This estimated pressure gradient may then be used to estimate the acoustic intensity in the frequency domain as

$$\widehat{\mathbf{I}}_c = \frac{j}{\rho_0\omega}p_0\widehat{\nabla p}^*, \tag{2.7}$$

where $p_0 = p(\mathbf{r}_0)$ is the pressure at the"center of mass" of the probe, and

$$\mathbf{r}_0 = \frac{1}{N}\sum_{i=1}^{N}\mathbf{r}_i. \tag{2.8}$$

The work of Wiederhold *et al.*[35,36,40] gives a detailed analysis of optimal methods of finding p_0 given different probe configurations. In these works, Wiederhold *et al.* discuss different finite-sum and finite-difference processing methods and their associated biases. Unless a microphone exists at the center of a probe configuration, these methods must be referenced to attain optimal intensity estimates for a given probe configuration. If a microphone exists at the center of the probe, such as in the probe used by Miah *et al.*,[41] p_0 is the complex pressure measured by the center microphone.

2.2.3 Phase and amplitude gradient estimation (PAGE) method

The new phase and amplitude gradient estimation (PAGE) method uses estimates of the phase gradient and amplitude gradient of a pressure field to estimate the acoustic intensity. The PAGE method is most easily developed using the notation of Mann and Tichy. First, the complex pressure is separated into amplitude and phase components,

$$p(\mathbf{r}) = P(\mathbf{r})e^{-j\phi(\mathbf{r})}, \tag{2.9}$$

where P and ϕ are real, scalar functions of the position $\mathbf{r}$, representing the amplitude and phase of the pressure respectively. The gradient of the pressure p can be written in terms of P and ϕ as

$$\nabla p(\mathbf{r}) = [\nabla P(\mathbf{r}) - jP(\mathbf{r})\nabla\phi(\mathbf{r})]\, e^{-j\phi(\mathbf{r})}. \tag{2.10}$$

The active and reactive components of the intensity can be rewritten as

$$\mathbf{I}_a = \frac{1}{\omega\rho_0} P^2 \nabla\phi, \tag{2.11a}$$

$$\mathbf{I}_r = -\frac{1}{\omega\rho_0} P\nabla P. \tag{2.11b}$$

We now can obtain an estimate of $\mathbf{I}$ from estimates of P, $\nabla\phi$, and ∇P.

First, using the same least-squares estimate as Eq. (2.6), $\nabla\phi$ is estimated as

$$\widehat{\nabla\phi} = \left(\mathbf{X}^T\mathbf{X}\right)^{-1}\mathbf{X}^T\boldsymbol{\Delta}\phi. \tag{2.12}$$

where $\boldsymbol{\Delta}\phi$ represents a vector of pairwise phase differences, which must be obtained from the measurements of pressure. The phase difference between two sensors can be found from the transfer function

$$\phi(\mathbf{r}_j) - \phi(\mathbf{r}_i) = \arg\left\{e^{j(\phi(\mathbf{r}_j)-\phi(\mathbf{r}_i))}\right\} \tag{2.13}$$

$$= -\arg\left\{e^{-j(\phi(\mathbf{r}_j)-\phi(\mathbf{r}_i))}\right\} \tag{2.14}$$

$$= -\arg\left\{\frac{p_j}{p_i}\right\} \tag{2.15}$$

$$= -\arg\left\{H_{ji}\right\}. \tag{2.16}$$

Thus the vector of pairwise phase differences, $\boldsymbol{\Delta}\phi$, is given by the pairwise transfer functions as follows:

$$\boldsymbol{\Delta}\phi = -\begin{bmatrix} \arg\{H_{12}\} \\ \arg\{H_{13}\} \\ \vdots \\ \arg\left\{H_{N-1,N}\right\} \end{bmatrix}. \tag{2.17}$$

Because the phase differences can be obtained directly from the transfer functions, it is preferable to estimate $\nabla\phi$ using the method presented in Section 2.2.1 rather than using a least-squares estimate of the total phase ϕ, which would require the application of the arg function directly to the pressure measurements p_i to obtain the value of ϕ at each sensor location.

Next, the pressure amplitudes are found by taking the magnitudes of the measured complex pressures,

$$P_i = |p_i|. \tag{2.18}$$

∇P can be estimated using the same least-squares estimate as the previous gradients,

$$\widehat{\nabla P} = \left(\mathbf{X}^T\mathbf{X}\right)^{-1}\mathbf{X}^T\mathbf{\Delta}P, \tag{2.19}$$

where $\mathbf{\Delta}P$ represents all the pairwise differences of the estimated pressure amplitudes (P_i),

$$\mathbf{\Delta}P = \begin{bmatrix} P_2 - P_1 \\ P_3 - P_1 \\ \vdots \\ P_N - P_{N-1} \end{bmatrix}. \tag{2.20}$$

The pressure amplitude at the center of the probe must also be found. If there is a microphone at the center of the probe, P_0 is found by taking the magnitude of the complex pressure of the center microphone. If a configuration without a center microphone is used, an analysis similar to the work of Wiederhold *et al.* must be employed.[35,36,40]

Using these estimated quantities, we can now estimate the reactive and active intensities as

$$\widehat{\mathbf{I}}_a = \frac{1}{\omega\rho_0}P_0^2\widehat{\nabla\phi} \tag{2.21a}$$

$$\widehat{\mathbf{I}}_r = -\frac{1}{\omega\rho_0}P_0\widehat{\nabla P}. \tag{2.21b}$$

2.2.4 Phase unwrapping

Multi-microphone intensity probes are generally limited to an upper frequency limit, determined by the separation distance between microphones. This limit, which we will call the spatial Nyquist limit, occurs when $kd = \pi$, where k is the wavenumber, and d is the separation distance between microphones. The FD method suffers from a frequency-dependent bias, where the intensity magnitude is underestimated as kd approaches π. Past the spatial Nyquist limit, the direction and the magnitude of the intensity estimates given by the FD method become completely unreliable. While the PAGE method does not suffer from the same inherent frequency-dependent bias as the FD method, it still normally gives incorrect estimates past the spatial Nyquist limit. Given certain measurement source characteristics, this limit can be surpassed by unwrapping the phase differences in the argument of the transfer functions.

The phase differences used in the PAGE method are found by taking the argument of the transfer functions between microphones, $\arg\{H_{ij}\}$. The argument function is limited between $-\pi$ and π, and as such, when the phase function between two microphones is greater than $\pm\pi$ the phase function will wrap. For example, a phase difference of 1.1π will wrap to $-.9\pi$. The phase difference between microphones will equal $\pm\pi$ when half the acoustic wavelength is equal to the separation distance between the microphones, also known as the spatial Nyquist limit. These wrapped phase differences result in incorrect phase gradients and thus provide meaningless intensity estimates. When measuring a broadband response, the phase differences function in the frequency domain will be continuous up to the spatial Nyquist limit. At this point, the phase function will wrap and exhibit a $\pm 2\pi$ jump. If we use a simple "unwrap" function, this discontinuity can be corrected by adding $\pm 2\pi$ to the phase function in frequencies above the discontinuity. Because this type of unwrapping requires a continuous phase function, a broadband source is required. This phase function unwrapping allows for accurate phase gradient components past the spatial Nyquist limit, which in turn allows for accurate intensity estimates well past the spatial Nyquist limit.

With a noise free measurement, there is no upper frequency limit to the PAGE method if the phase function is unwrapped. In practice, noise in the argument of the transfer function will limit the extent to which the phase function can be unwrapped. A noisy transfer function will cause the argument of the transfer function to have multiple discontinuities when the function approaches the $\pm\pi$ limit. If just one of the occurring 2π jumps is not correctly accounted for, the entire function past that frequency will be incorrect. Thus, minimizing the noise in the transfer functions allows for a larger range of correctly unwrapped phase differences and thus a larger range of accurate intensity estimates. The primary means of minimizing noise in the transfer function is through ensemble averaging, which is discussed in the next section.

2.2.5 Averaging

When applying either the FD or the PAGE method to physical data, it can be advantageous to apply averaging, especially with non-repeatable noise sources. The averaging required for the FD method is relatively simple: the time waveform is broken into blocks, and then the complete intensity processing as discussed above is applied to each block. Each block will then have an associated intensity vector. The average of these vectors is the complete averaged intensity. This approach will provide the same result as averaging the individual cross-spectra and then computing the intensity estimates.

Because the PAGE method relies on the phase of the transfer function, the order of operations with ensemble averaging must be more carefully considered. To obtain the most accurate time-averaged intensity, the transfer functions, H_{12}, H_{13}, etc., of each block are calculated. These transfer functions are then averaged, and the averaged transfer functions are used in the PAGE calculations. For example,

$$H_{12,\text{avg}} = \frac{1}{N}\sum_{n=1}^{N} H_{12,n}, \tag{2.22}$$

where N is the total number of blocks, and n represents the index of each block. The argument

of these averaged transfer functions is then used in the PAGE method calculations and result in $\widehat{\nabla\phi}_{\text{avg}}$. Similarly, the pressure amplitudes $P_{i,\text{avg}}$ can be found by calculating P_i for each block and taking the mean. The averaged pressure amplitudes are then used to calculate $\widehat{\nabla P}_{\text{avg}}$ using the same method outlined earlier. The quantities $P_{i,\text{avg}}$, $\widehat{\nabla P}_{\text{avg}}$ and $\widehat{\nabla\phi}_{\text{avg}}$ are then combined to create a single averaged intensity estimate.

As discussed in Section 2.2.4, the upper frequency limit of the unwrapped PAGE method will depend on the noise in the argument of the transfer functions between microphones. Ensemble averaging, as discussed here, helps smooth the transfer functions, and helps the phase to be unwrapped at higher frequencies. The trade-off with ensemble averaging is that the spectral resolution decreases as the number of averages increases.

2.3 Comparison of FD and PAGE intensity estimates

We now compare the accuracy of the intensity estimates produced by the finite-difference method to those produced by the PAGE method. First, we consider a one-dimensional intensity probe with two ideal microphones separated by a distance, d, in a plane wave of axial incidence. Given the pressure from a plane wave traveling in the x direction,

$$p(x) = Ae^{-jkx}, \tag{2.23}$$

where A is the acoustic pressure amplitude and k is the wavenumber, the intensity of the wave is

$$\mathbf{I}(x) = \frac{k|A|^2}{\rho_0 \omega}\hat{\mathbf{x}}, \tag{2.24}$$

where ω is the angular frequency, ρ_0 is the fluid mass density, and $\hat{\mathbf{x}}$ is a unit vector in the x direction. Given two microphones at locations

$$r_1 = -\frac{d}{2}, \quad r_2 = \frac{d}{2}, \tag{2.25}$$

the literature shows that the FD method estimates the intensity as

$$\hat{\mathbf{I}}_a^{\mathrm{FD}} = -\frac{1}{\omega\rho_0 d}\mathrm{Im}\{S_{12}(\omega)\}\hat{\mathbf{x}}, \tag{2.26}$$

where S_{ij} represents the cross-spectrum of the two complex pressure measurements.[21] This same result can be obtained using the method given in Section 2.2.2

$$\hat{\mathbf{I}}_c^{\mathrm{FD}} = \frac{j}{\omega\rho_0}\left(\frac{p_1+p_2}{2}\right)\left(\frac{p_2-p_1}{d}\right)^*\hat{\mathbf{x}} \tag{2.27}$$

$$= \frac{j}{2\omega\rho_0 d}(p_1p_2^* - p_1p_1^* + p_2p_2^* - p_2p_1^*)\hat{\mathbf{x}}. \tag{2.28}$$

Taking the real part of this equation and representing the cross spectrum as S_{ij} gives us

$$\hat{\mathbf{I}}_a^{\mathrm{FD}} = \frac{1}{2\omega\rho_0 d}\mathrm{Re}\{j(S_{12} - |p_1| + |p_2| - S_{21})\}\hat{\mathbf{x}}. \tag{2.29}$$

This equation simplifies to Eq. (2.26) since $|p_1| = |p_2|$ for a plane wave. This expression provides an accurate approximation for intensity at low values of kd, but underestimates the intensity as kd approaches π.

Using the results of Section 2.2.3, the estimate given by the PAGE method is calculated as

$$\hat{\mathbf{I}}^{\mathrm{PAGE}} = \frac{-\arg\{H_{12}\}}{\omega\rho_0 d}\left(\frac{|p_1|+|p_2|}{2}\right)^2\hat{\mathbf{x}}. \tag{2.30}$$

This equation simplifies to

$$\hat{\mathbf{I}}^{\mathrm{PAGE}} = \frac{-\arg\{H_{12}\}}{\omega\rho_0 d}|A|^2\hat{\mathbf{x}} \tag{2.31}$$

because $|p_1| = |p_2| = |A|$ for a plane wave. The phase of a plane wave is given by kx, so the difference of phases of two microphones, $-\arg(H_{12})$, separated a distance d will simplify to kd, as long as $kd < \pi$, which is the spatial Nyquist limit of the probe. Within this limit, the expression for the intensity simplifies to

$$\hat{\mathbf{I}}^{\mathrm{PAGE}} = \frac{kd}{\omega\rho_0 a}|A|^2 \tag{2.32}$$

$$= \frac{k|A|^2}{\rho_0\omega}, \qquad (kd < \pi) \tag{2.33}$$

which is the exact expression for the intensity of a plane wave as seen in Eq. (2.24). Simply put, an intensity probe with two ideal microphones can perfectly estimate intensity in one dimension with the PAGE method as long as $kd < \pi$. Furthermore, if phase unwrapping is applied (Section 2.2.4), there is no frequency limit for the one-dimensional PAGE method applied to plane waves. Figure 2.1 shows the magnitude of the error in estimating the plane wave with both the FD and PAGE methods. It can be seen that the PAGE method significantly outperforms the FD at all but the lowest values of ka. The PAGE method produces estimates with no error below the spatial Nyquist limit, and if phase unwrapping is used, the PAGE method would have no error for any value of ka.

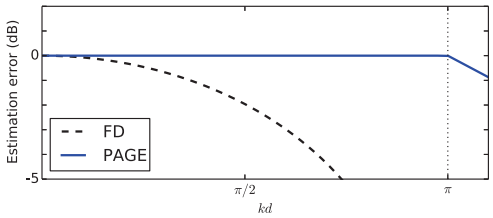

Figure 2.1: FD and PAGE estimation error given an ideal two-microphone sound intensity probe in a plane wave of axial incidence. The x axis is shown in terms of kd, where k is the wavenumber and d is the separation distance between the microphones. Phase unwrapping is not applied to the PAGE estimate.

We now consider intensity estimates in multiple dimensions. This is accomplished by comparing analytically derived intensities of two-dimensional fields to intensity estimates of the same fields given a two-dimensional, four-microphone probe. Two fields are considered: a plane wave and a three source system. Both pressure fields considered have reflection symmetry, and the probe is confined to the plane of reflection. First, the derivation of the intensity expressions generated by the FD and PAGE methods for a two-dimensional probe is demonstrated.

2.3.1 FD and PAGE expressions for a two-dimensional probe

The chosen probe geometry is an equilateral triangle with a sensor at the center. This is similar to the design evaluated by Suzuki *et al.*,[42] except that the center microphone is lowered so that all the microphones are in the same plane. Each of the outside microphones is placed 2 inches from the center microphone. Using this geometry, p_0 and P_0 can be determined from the center microphone. It must be noted that without a sensor in the center of the probe, the approach developed by Wiederhold *et al.*[35,36,40] must be employed.

If a is the radius of the circle that circumscribes the probe, then the two-dimensional position vectors of the probe sensors relative to the probe center are

$$\mathbf{r}_1 = \begin{bmatrix} 0 \\ 0 \end{bmatrix}, \quad \mathbf{r}_2 = a \begin{bmatrix} 0 \\ 1 \end{bmatrix},$$
$$\mathbf{r}_3 = \frac{a}{2} \begin{bmatrix} \sqrt{3} \\ -1 \end{bmatrix}, \quad \mathbf{r}_4 = -\frac{a}{2} \begin{bmatrix} \sqrt{3} \\ 1 \end{bmatrix}, \tag{2.34}$$

and the matrix, $\mathbf{X}$, is

$$\mathbf{X} = \begin{bmatrix} (\mathbf{r}_2 - \mathbf{r}_1)^T \\ (\mathbf{r}_3 - \mathbf{r}_1)^T \\ (\mathbf{r}_4 - \mathbf{r}_1)^T \\ (\mathbf{r}_3 - \mathbf{r}_2)^T \\ (\mathbf{r}_4 - \mathbf{r}_2)^T \\ (\mathbf{r}_4 - \mathbf{r}_3)^T \end{bmatrix} = \frac{a}{2} \begin{bmatrix} 0 & 2 \\ \sqrt{3} & -1 \\ -\sqrt{3} & -1 \\ \sqrt{3} & -3 \\ -\sqrt{3} & -3 \\ -2\sqrt{3} & 0 \end{bmatrix}. \tag{2.35}$$

The pressure gradient as estimated by the FD method is

$$\widehat{\nabla p} = \frac{1}{3a} \begin{bmatrix} \sqrt{3}(p_3 - p_4) \\ 2p_2 - p_3 - p_4 \end{bmatrix}. \tag{2.36}$$

Since p_1 is at the center of the probe, p_0 is equal to p_1, and the estimated complex intensity is given by Eq. (2.7)

$$\begin{aligned}\widehat{\mathbf{I}}_c^{\mathrm{FD}} &= p\mathbf{u}^* \\ &= p_1(\frac{j}{\rho_0\omega}\widehat{\nabla p})^* \\ &= \frac{-j}{3\rho_0\omega a}\begin{bmatrix}\sqrt{3}(p_1p_3^* - p_1p_4^*) \\ 2p_1p_2^* - p_1p_3^* - p_1p_4^*\end{bmatrix},\end{aligned} \tag{2.37}$$

or in terms of the one-sided cross-spectrum $G_{ij} = 2p_i^* p_j$

$$\widehat{\mathbf{I}}_c^{\mathrm{FD}} = \frac{-j}{6\rho_0\omega a}\begin{bmatrix}\sqrt{3}(G_{31} - G_{41}) \\ 2G_{21} - G_{31} - G_{41}\end{bmatrix}. \tag{2.38}$$

In the PAGE method, the pairwise pressure differences used in the FD method are replaced by the argument of pairwise transfer functions. As was shown previously, this is equivalent to the pairwise phase differences. The estimated phase gradient is

$$\widehat{\nabla\phi} = -\frac{1}{3a}\begin{bmatrix}\sqrt{3}\arg\{H_{34}\} \\ \arg\{H_{23}\} + \arg\{H_{24}\}\end{bmatrix}. \tag{2.39}$$

The estimated pressure amplitude gradient is

$$\widehat{\nabla P} = \frac{1}{3a}\begin{bmatrix}\sqrt{3}(P_3 - P_4) \\ 2P_2 - P_3 - P_4.\end{bmatrix}. \tag{2.40}$$

The pressure amplitude at the probe center is $P_0 = P_1 = |p_1|$. The active and reactive components of acoustic intensity are then estimated by the PAGE method as

$$\widehat{\mathbf{I}}_a^{\mathrm{PAGE}} = -\frac{P_1^2}{6a\omega\rho_0}\begin{bmatrix}\sqrt{3}\arg\{H_{34}\} \\ \arg\{H_{23}\} + \arg\{H_{24}\}\end{bmatrix}, \tag{2.41}$$

$$\widehat{\mathbf{I}}_r^{\mathrm{PAGE}} = -\frac{P_1}{6a\omega\rho_0}\begin{bmatrix}\sqrt{3}(P_3 - P_4) \\ 2P_2 - P_3 - P_4\end{bmatrix}. \tag{2.42}$$

We consider the application of the expressions given in Eqs. (2.37), (2.41), and (2.42) to ideal fields. It should be noted that instead of explicitly calculating the estimated intensity in terms of cross-spectra and transfer functions, it can be simpler to leave the derivations in terms of component matrices and vectors. For example, once P_0, $\mathbf{\Delta}\phi$, and $\mathbf{X}$ are known, Eq. (2.41) can be computed in one line as

$$\widehat{\mathbf{I}}_a^{\text{PAGE}} = \frac{1}{\omega\rho_0} P_0^2 \left(\mathbf{X}^T\mathbf{X}\right)^{-1} \mathbf{X}^T \mathbf{\Delta}\phi. \tag{2.43}$$

2.3.2 Plane wave

Using the expressions developed previously, we again investigate estimation error of a plane wave. Two quantities are used to evaluate the accuracy of the estimation methods: the error in the amplitude

$$|\mathbf{I}|^{\%\text{err}} = 100\frac{||\hat{\mathbf{I}}| - |\mathbf{I}||}{|\mathbf{I}|} \tag{2.44}$$

and the angle between the estimated and exact intensity vectors

$$\theta^{\text{err}} = \arccos\frac{\hat{\mathbf{I}}\cdot\mathbf{I}}{|\hat{\mathbf{I}}||\mathbf{I}|}. \tag{2.45}$$

The results are presented in Figs. 2.2 and 2.3. The error is shown using shades of gray to represent error ranges; all white regions correspond to less than 1% error in amplitude (Fig. 2.2) or less than 0.01° in error in the estimated direction (Fig. 2.3). All black regions correspond to amplitude error greater than 30% or error in the estimated direction greater than 1°. The various shades of gray correspond to intermediate ranges.

Figure 2.2 shows the error in the intensity magnitude estimated with the FD (part a) and PAGE (part b) methods, where no phase unwrapping is applied to the PAGE method. It can be seen that both methods break down past the spatial Nyquist point, where the wavelength of the impinging plane wave becomes equal to the largest microphone separation distance parallel to the direction of wave propagation. This occurs near $kd = \pi$, where d is the maximum microphone separation

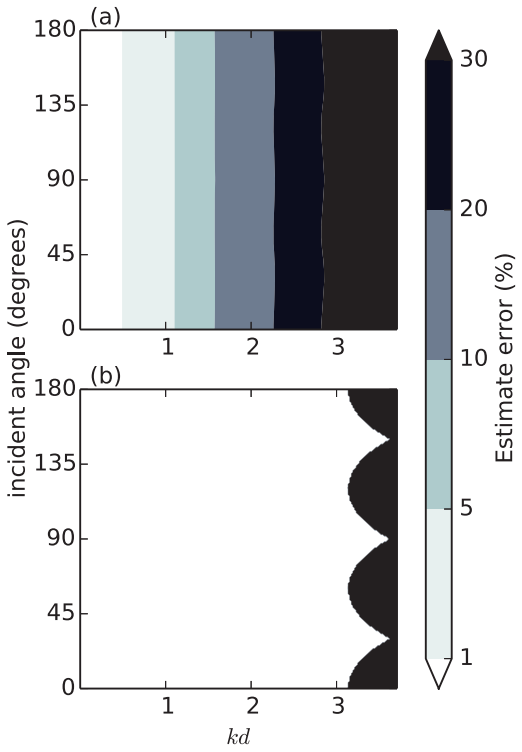

Figure 2.2: The intensity amplitude estimation error of the FD (a) and PAGE (b) methods as functions of probe rotation angle θ (measured in degrees) and kd, where k is the wavenumber, and d is the maximum microphone separation distance within the probe.

distance. Since the largest sensor separation distance parallel to the impinging wave depends on rotation, this limit varies, as can be seen in Fig. 2.2(b). If phase unwrapping is used with the PAGE method, it will no longer break down at the spatial Nyquist limit and will result in negligible error over all frequencies. The frequency bias inherent to the FD method is apparent, where the estimation error increases as frequency increases. While this bias is reduced by using the center microphone for the pressure component of intensity,[40] it can still be clearly seen in Fig. 2.2 where the estimation error of the FD method increases as kd increases. The PAGE method does not suffer from this same bias as it gives accurate estimates up to the spatial Nyquist limit of the probe. Thus

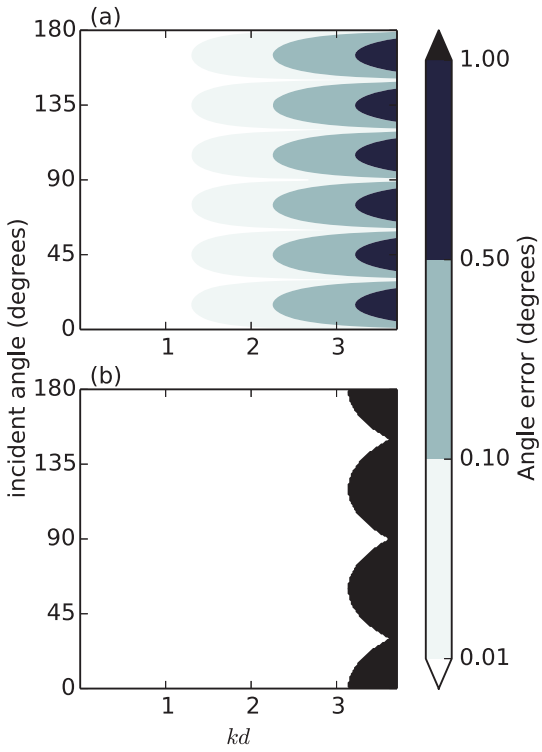

Figure 2.3: Error in the estimated angle of the acoustic intensity. The error in the angles estimated by the FD (a) and PAGE (b) methods as functions of probe rotation angle θ (measured in degrees) and kd, where k is the wavenumber, and d is the maximum microphone separation distance within the probe.

we see that for propagating plane wave fields measured by the 2D probe in question, the PAGE method provides better intensity estimates. Though the results are only shown for a particular probe configuration, similar results can be seen with other probe types.

2.3.3 Three-source system

A more complicated acoustic intensity field can be created with three evenly spaced monopoles on a line, with the middle monopole 180° out of phase with the other two. The pressure at any field

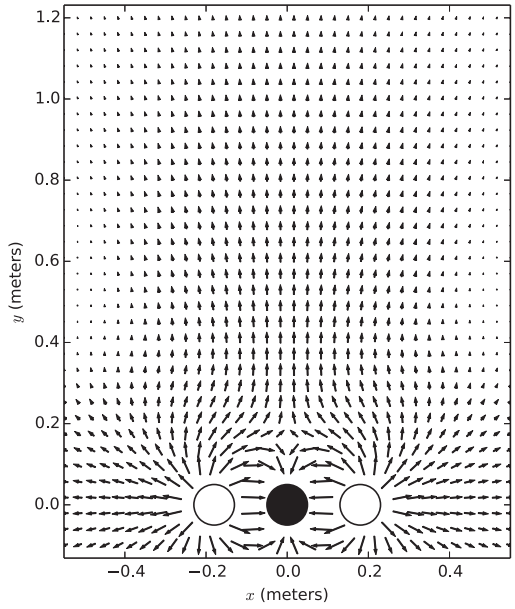

Figure 2.4: Active intensity produced by a system of three simple sources spaced evenly on a line, with the center source 180° out of phase with the others. The frequency is 400 Hz, and the sources are spaced 18 cm apart.

point is

$$p(\mathbf{r}) = \sum_{i=1}^{3} A_i \frac{e^{-jk|\mathbf{r}-\mathbf{r}_i|}}{|\mathbf{r}-\mathbf{r}_i|} \tag{2.46}$$

where $A_1 = 1\,\mathrm{Pa}\cdot\mathrm{m}$, $A_2 = -1\,\mathrm{Pa}\cdot\mathrm{m}$, $A_3 = 1\,\mathrm{Pa}\cdot\mathrm{m}$ and $\mathbf{r}_1 = [-0.18, 0, 0]^{\mathrm{T}}\mathrm{m}$, $\mathbf{r}_2 = [0,0,0]^{\mathrm{T}}\mathrm{m}$, $\mathbf{r}_3 = [0.18, 0, 0]^{\mathrm{T}}\mathrm{m}$. The particle velocity is

$$\mathbf{u}(\mathbf{r}) = \sum_{i=1}^{3} -j \frac{A_i}{k\rho_0 c_0} \frac{\mathbf{r}-\mathbf{r}_i}{|\mathbf{r}-\mathbf{r}_i|^3} \left(1 + jk|\mathbf{r}-\mathbf{r}_i|\right) e^{-jk|\mathbf{r}-\mathbf{r}_i|}. \tag{2.47}$$

Figure 2.4 shows the active acoustic intensity of this field. The expressions for the estimated active intensities given in Eqs. (2.37) and (2.41) are used to predict the intensities over the domain shown, and the error of these estimates (given by Eqs. (2.44) and (2.45)) is presented in Figs. 2.5 and 2.6. By looking at the estimation errors of this complicated intensity field, we can determine how both

the methods presented perform in complicated fields. In the near field of these monopoles there will be significant reactive components of the intensity, but the evaluation of the PAGE and FD method for reactive intensities is not considered at this time. The probe used to evaluate these fields has a microphone separation distance (a) of 5.08 cm (2 in.), which results in a maximum separation distance, d, of 8.8 cm. The frequency being evaluated is 400 Hz, which leads to a kd of 0.645. Shades of gray again represent error ranges. The range of errors for this field is greater than in the case of the plane wave and so the error ranges are larger.

The black regions near the sources indicate that both the FD and PAGE methods fail to accurately represent the acoustic intensity in these regions. It is clear that away from the complicated near field of the three monopoles, both methods give reasonable results for the active intensity. However, the PAGE method gives more accurate results than the FD method across most of the near field. These figures only show results at a single frequency, but a similar pattern is seen over all frequencies: the PAGE method consistently outperforms the FD method.

.

2.4 Error analysis

Both the FD and PAGE methods rely on phase-matched microphones. At low frequencies, even small phase errors between microphones cause large errors in intensity estimates. Phase calibration of microphones can help minimize the errors caused by phase mismatch. In addition, the impact of phase mismatch is lessened when the distance between microphones is increased.

At high frequencies, sound scattering off the body of an intensity probe can cause errors in acoustic intensity. This can be reduced by minimizing the scattering surfaces of the probe and by increasing the separation distance between microphones. However, the spatial Nyquist limit is proportional to the inverse of the separation distance, and so increasing microphone separation

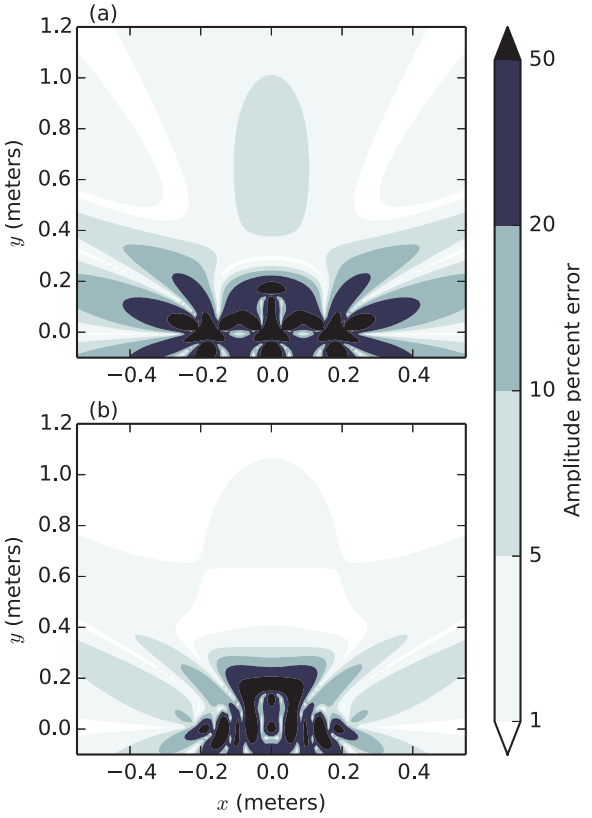

Figure 2.5: Error in the estimated magnitude of the active intensity at 400 Hz of the three-source system shown in Fig. 2.4 for the FD (a) and PAGE (b) methods. Estimates are calculated using the two-dimensional probe described in Eq. (2.35)

reduces the spatial Nyquist limit. This has led to most acoustic intensity probes employing closely spaced microphones, thus sacrificing lower frequencies for a larger frequency range. As discussed in Section 2.2.4, the phase components of the PAGE method can be unwrapped, and accurate results can be obtained beyond the spatial Nyquist limit in appropriate fields. Using this phase unwrapping, larger separation distances can be used without sacrificing higher frequencies. Thus, the problems of both phase mismatch at low frequencies and scattering at high frequencies can be mitigated by increasing the microphone separation. The size of an intensity probe using the PAGE

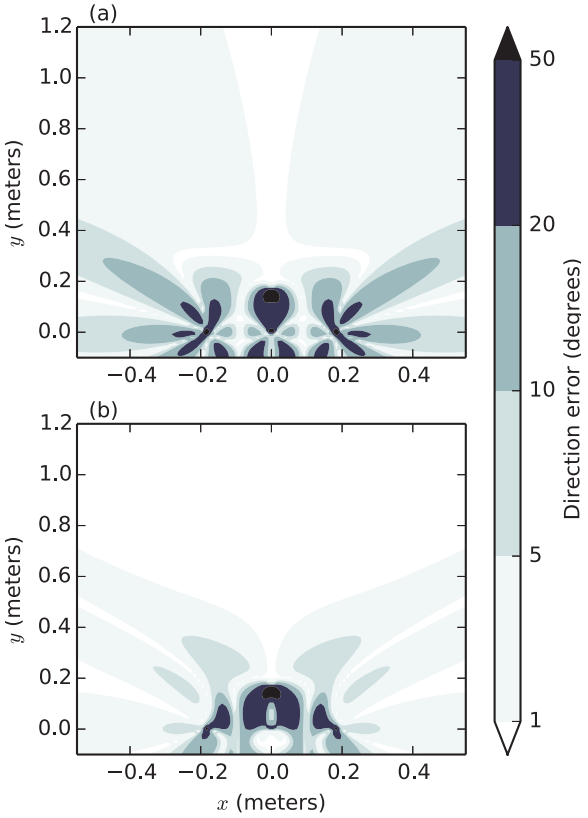

Figure 2.6: Error in the estimated direction of the active intensity for the three-source system shown in Fig. 2.4 for the FD (a) and PAGE (b) methods. Estimates are calculated using the two-dimensional probe described in Eq. (2.35).

method still needs to remain small enough that the field is locally planar.

2.4.1 Uncertainty analyses

As the PAGE method is new, the following section will give a more complete example of how small phase errors affect acoustic intensity errors. For this section, we will be using overbars to denote actual values, so for example, if p is the measured pressure, $\bar{p}$ would be the actual pressure.

First, we will assume that the measurable pressure amplitude and phase are both random variables normally distributed about their physical values, so

$$P \sim \mathcal{N}(\bar{P}, \sigma_P^2) \tag{2.48}$$

and

$$\phi \sim \mathcal{N}(\bar{\phi}, \sigma_\phi^2). \tag{2.49}$$

The complex pressure can then be simulated by combining these two random variables

$$p = Pe^{j\phi}. \tag{2.50}$$

By assuming the different phase and amplitude random variables are independent, the difference between these will also be normally distributed. Thus we can write the vectors of phase and amplitude differences as

$$\mathbf{\Delta}\phi \sim \mathcal{N}(\overline{\mathbf{\Delta}\phi}, \sigma_{\mathbf{\Delta}\phi}^2) \tag{2.51}$$

and

$$\mathbf{\Delta}P \sim \mathcal{N}(\overline{\mathbf{\Delta}P}, \sigma_{\mathbf{\Delta}P}^2), \tag{2.52}$$

Furthermore, because of the assumed independence, we know that

$$\sigma_{\mathbf{\Delta}\phi}^2 = 2\sigma_\phi^2 \tag{2.53}$$

and

$$\sigma_{\mathbf{\Delta}P}^2 = 2\sigma_P^2. \tag{2.54}$$

Following the work of Szuberla *et al.*,[43] we can now find the variance in the gradient of the phase and amplitude by defining

$$\mathbf{C} = \mathbf{X}^T\mathbf{X}, \tag{2.55}$$

$$\mathbf{D} = \mathbf{E}^T \mathbf{C}\mathbf{E} = \begin{bmatrix} \lambda_1 & 0 & \cdots & 0 \\ 0 & \lambda_2 & & \\ \vdots & & \ddots & \vdots \\ 0 & & \cdots & \lambda_n. \end{bmatrix}, \tag{2.56}$$

where $\mathbf{C}$ is the sensor separation covariance matrix, $\mathbf{E}$ is a matrix of eigenvectors of $\mathbf{C}$, and $\mathbf{D}$ is a diagonal matrix of eigenvalues. The variances of the gradients can be written as

$$\sigma_{\nabla\phi,n} = \sqrt{\frac{\sigma^2_{\Delta\phi}}{\lambda_n}} \tag{2.57}$$

$$\sigma_{\nabla P,n} = \sqrt{\frac{\sigma^2_{\Delta P}}{\lambda_n}}, \tag{2.58}$$

where λ_n represents the eigenvalues in $\mathbf{D}$. The eigenvectors in $\mathbf{E}$ define the rotation of the coordinates from the principal axis. Thus we can represent the phase and amplitude gradients in terms of multivariate Gaussians, centered at the location of the actual values with covariance defined by $\mathbf{C}$. These can be combined with the Gaussian pressure amplitudes to simulate the intensity as

$$\mathbf{I}_a^{PAGE} = \frac{1}{\omega\rho_0} P^2 \nabla\phi \tag{2.59}$$

$$\mathbf{I}_r^{PAGE} = -\frac{1}{\omega\rho_0} P \nabla P, \tag{2.60}$$

where

$$P \sim \mathcal{N}(\bar{P}, \sigma_P^2), \tag{2.61}$$

and

$$\nabla\phi \sim \mathcal{N}(\overline{\nabla\phi}, \mathbf{C}_{\nabla\phi}), \tag{2.62}$$

$$\nabla P \sim \mathcal{N}(\overline{\nabla P}, \mathbf{C}_{\nabla P}). \tag{2.63}$$

We can now simulate the uncertainties associated with determined phase and amplitude errors. For the following figures the same 2D intensity probe from Section 2.3.1 is used, and we assume

typical calibration errors of $\sigma_P = 0.05$ dB and $\sigma_\phi = 0.05^\circ$. This means that the input pressures are 95% accurate within ± 0.1 dB and $\pm 0.1^\circ$. Frequency independent calibration errors are used for this analysis, though it should be noted that in practice phase mismatch is likely to be worse at low-frequencies.

Using these sigma values, a random set of normally distributed pressure amplitudes P and phase values ϕ are generated. The FD and PAGE methods are then applied to the generated values to estimate the intensity. If we assume the resulting PAGE and FD estimates are multivariate normal distributions, we can estimate the covariance matrix associated with the scattered intensities.[44] This covariance matrix, along with the mean of the resulting intensities, is used to find a 95% ellipse to fit the data. Using more points has negligible effect on the resulting error ellipses, so it is determined that 10,000 intensity estimates is a sufficient sample size. The resulting 95% error ellipses can be seen in Fig. 2.7. As we can see in the figure, measurement uncertainties of the PAGE and FD methods are nearly equivalent at low frequencies. At higher frequencies, the frequency-dependent bias of the FD method can be see as the error ellipse is no longer centered around the correct value, but instead the intensity is underestimated.

One insight gained from Fig. 2.7 is how each method responds to calibration. The magnitude of the uncertainties found through the PAGE method are correlated directly with magnitude calibration errors. For example, increasing σ_P results in larger magnitude uncertainties but has no effect on the angle uncertainties. The uncertainty ellipses from the FD method, on the other hand, do not seem to have as direct of a correlation; increasing σ_P affects both the phase and magnitude errors.

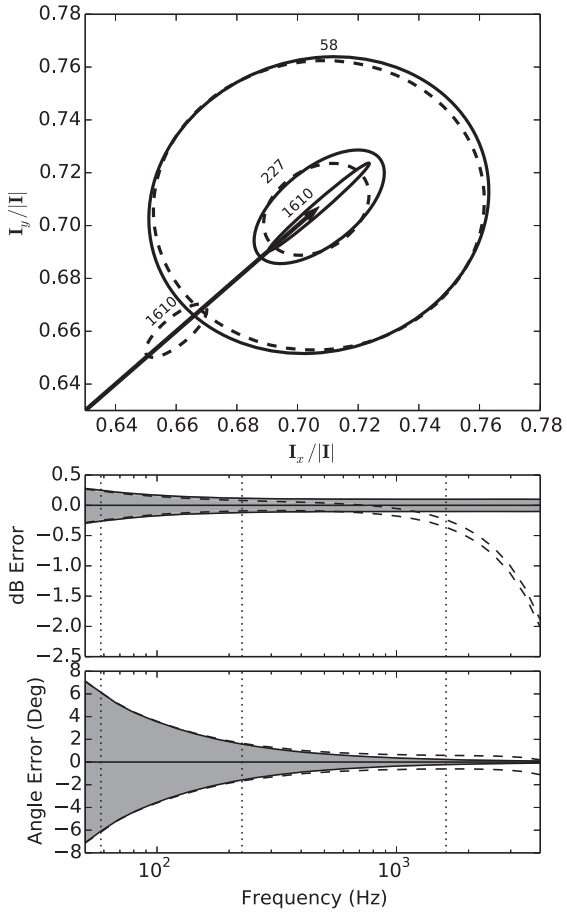

Figure 2.7: Uncertainty in magnitude and direction of the intensity found from the 95% confidence ellipses for both the FD (dashed lines, no fill) and PAGE (solid lines, gray fill) methods. Uncertainties are calculated using the the two-dimensional probe described in Eq. (2.35), and using calibrations errors of $\sigma_P = 0.05$ dB and $\sigma_\phi = 0.05^\circ$. The plot on the top shows three sample error ellipses at frequencies marked by dotted vertical lines on the bottom two plots. The vector in the top plot represents the analytic intensity.

2.5 Summary and conclusions

We have presented a least-squares formulation of the gradient estimation technique for arbitrary probe geometries. This method has been applied to the finite-difference p-p (FD) method for

estimating the acoustic intensity. We also developed a new technique that we have termed the phase and amplitude gradient estimation (PAGE) method by combining finite-difference estimates for the phase and amplitude gradients with the analytical work of Mann and Tichy.[2,37,38] This method estimates $\nabla\phi$ and ∇P separately and uses the result to estimate the acoustic intensity. The estimated phase gradient $\widehat{\nabla\phi}$ is obtained from the pairwise transfer functions of the microphones in the probe. The amplitude gradient $\widehat{\nabla P}$ is estimated using the resulting pairwise differences of the pressure amplitudes measured at the microphones in the probe. One advantage of the PAGE method is that the estimated phase gradient can be unwrapped in certain cases, which allows for accurate intensity estimates past the spatial Nyquist limit. Special consideration was given when using ensemble averaging with the PAGE method.

The FD and PAGE methods have been compared for three cases: a one-dimensional probe in a plane-wave field, a two-dimensional probe rotated in a plane-wave field, and the two-dimensional probe in the field produced by three ideal point sources. These cases have been chosen to illustrate the advantages of the PAGE method for estimating the acoustic intensity of plane-wave fields and to show that the advantages persist in more complex systems. It has been shown that for all these cases, the PAGE method estimates exhibit less error than the FD method estimates. The PAGE method produces estimates of the active acoustic intensity with negligible error for plane-wave fields with frequencies below the spatial Nyquist frequency. Furthermore, in the case of the three-source system presented in Fig. 2.4, the PAGE method has less overall error than the FD method.

Finally, a brief error analysis of the FD and PAGE methods has been presented. It was shown that calibration errors have equal effects on both methods at low frequencies. However, the FD method produces significantly biased results at higher frequencies while the PAGE method has no bias. Furthermore, the robustness of the PAGE method at frequencies above the spatial Nyquist allows for the microphones to be spaced farther apart which in turn helps to improve the low frequency estimates.

The PAGE method developed here provides significant advantages over the standard finite-difference p-p method for estimating acoustic intensity. Because the PAGE method uses the same hardware as the FD method, the PAGE method can be implemented on any existing finite-difference p-p intensity probe. It does not suffer from the same frequency-dependent bias and appears to be more accurate in general.

Chapter 3

Laboratory validation

3.1 Introduction

In this chapter, we investigate the effectiveness of a new approach for the estimation of acoustic intensity, inspired by the work of Mann *et al.*[37] and Mann and Tichy.[2,38] Rather than estimate the pressure gradient directly from the complex pressures, this new method uses estimates of the gradients of the pressure phase and amplitude separately. We refer to this method as the phase and amplitude gradient estimation method, or the PAGE method. This new method has been shown to be analytically superior to the traditional method of estimating acoustic intensity, the finite-difference p-p method. The traditional finite-difference p-p method of estimating acoustic intensity will be referred to simply as the FD method for the remainder of the chapter.

A recent experiment was conducted to investigate and compare the PAGE method to the FD method. For this experiment, complicated acoustic intensity fields were created using two configurations of a loudspeaker array. First, a dipole response was created with two speakers close together with opposite phases. Second, a three-source system was made with three equally spaced speakers with the middle speaker having opposite phase of the outside speakers. Both these ar-

rangements create relatively complex acoustic intensity fields. A 2D plane directly in front of the speaker array was measured using an acoustic intensity probe that was developed specifically for rocket noise measurement. This is the same 2D probe arrangement discussed in Section 2.3.1.

To effectively evaluate the two intensity methods, we compare the measured intensities to a theoretical model. Point sources will be used to model the loudspeakers. Though this is an overly simplistic model, it provides a simple starting point for comparison.

3.2 Experimental setup

Two loudspeaker arrangements were used to create acoustic intensity fields. Both arrangements were chosen to create relatively complex acoustic intensity fields using a simple array of loudspeakers. The loudspeakers had a diameter of 2.5 in., and each was separated 7 in. from adjacent speakers.

First, a dipole-like field was created using two speakers with opposite phases. Second, a more complex field was generated by using three speakers in a line with the middle speaker 180° out of phase with the outside speakers. This was used to simulate a response like the one discussed in Section 2.3.3. Both arrangements were measured in an anechoic chamber. Coherent white noise was played into each speaker with the polarity switched on the 180° out of phase speakers. Using a scanning system, the 2D intensity probe was moved across a grid in front of the speaker array, and at each point in the grid the pressure at the microphones was measured. The FD and PAGE methods of estimating acoustic intensity were applied to the pressure data to find the frequency-dependent intensity at each location in the grid. The result is a 2D intensity map similar to those found in the article by Mann and Tichy.[2]

The primary advantage of the PAGE method is that it allows for accurate intensity measurements over a larger frequency band, as explained in Section 2.2. When measuring smoothly varying

broadband sources, it is possible to unwrap the phase component of the PAGE method, allowing for accurate intensity estimates well above the limitations of the FD method. This phase unwrapping is applied to the results.

To provide a comparison for the results, we must determine an expected intensity field given the source configurations. To determine the expected 2D intensity fields, we model the speakers in the array as monopoles. Though speakers are hardly point sources, this model should be sufficient for a qualitative comparison, particularly at lower frequencies where the acoustic wavelength is large compared to the loudspeaker diameter. The measured intensity fields are compared to the modeled intensities in the following section.

3.3 Results

Figures 3.1–3.8 seen at the end of this chapter compare the modeled intensities with the estimated intensities found from the FD and PAGE methods. The scanning system used for this experiment suffered from calibration errors which caused the x axis to drift. An attempt was made to correct for this drift in the processing, which is why the locations of the intensity vectors are skewed. The conclusions presented in this chapter serve primarily as a qualitative analysis. An extensive quantitative analysis of these results will be the subject of future work.

At low frequencies we can see that the estimates from both methods match the point-source model. This is demonstrated by comparing Fig. 3.1 with Fig. 3.2 and Fig. 3.5 with Fig. 3.6. We expect the model to match well at these low frequencies because the acoustic wavelength is large compared to the diaphragm of the loudspeakers, thus their response is similar to that of a point source. It appears that the PAGE method fails near the deep nulls of the dipole, possibly because one of the microphone lies directly in the null.

At higher frequencies we see large discrepancies between the PAGE and FD estimated inten-

sities. Figures 3.4 and 3.8 show that the measured intensity amplitudes from the FD method are significantly smaller than those of the PAGE method. Furthermore, the vector directions that result from the FD method are also clearly incorrect. Both the magnitude and direction errors in the FD estimates are a result of the frequency being past the spatial Nyquist limit of the probe. The PAGE method still performs decently at this frequency due to the unwrapped phase gradients. The magnitudes appear to be accurate, but the angles have errors in many areas of the fields. Comparing Fig. 3.3 with Fig. 3.4 and Fig. 3.7 with Fig. 3.8, we can see clearly that the point-source model no longer matches the estimated intensities. This is due to the acoustic wavelength (2.7 in.) being comparable to the diameter of the loudspeaker (2.5 in.), thus the monopole approximation in no longer as valid. Another concern is that at these higher frequencies the radius of curvature of the field may be comparable to the area of the probe. In other words the measured fields are no longer locally planar, which would cause errors in the intensity estimates. Using a smaller probe would be ideal for these spatially complex higher frequencies. It may also be possible to use the second-order methods discussed in Appendix A to be able to better resolve these complicated fields.

3.4 Conclusion

Qualitatively, we can clearly see that the PAGE method outperforms the FD method at high frequencies. Both methods appear to work well at low frequencies. With phase unwrapping, the PAGE method can be used past the spatial Nyquist limit to give intensity estimates well beyond the limits of the FD method. The systems created here are spatially complex at higher frequencies, and it is clear that this affects the PAGE method estimates. Even with the difficulties in resolving higher frequency fields, the PAGE method still clearly outperforms the FD method as it provides accurate magnitudes as well as somewhat accurate vector angles.

Future work will include taking a new data set to correct the errors due to the mis-calibrated scanning system. With this new data set, a rigorous quantitative comparison of the measured intensity fields to the modeled fields can be made, whereas this analysis has been primarily qualitative. A more accurate loudspeaker model may also be used to improve the high-frequency modeling. To further improve the model, the loudspeaker cone velocities can be measured as the data is taken, which can then be used as inputs into the improved model.

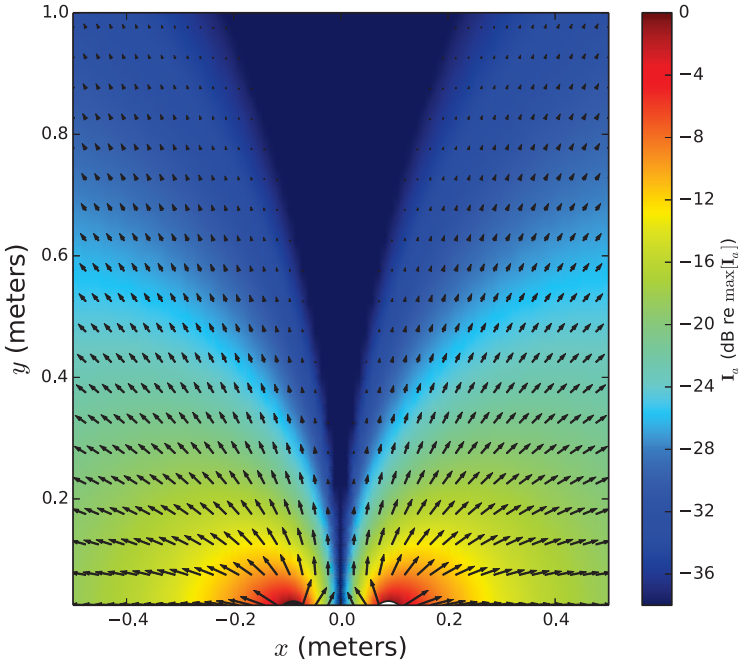

Figure 3.1: The modeled acoustic intensity field from two closely spaced, out-of-phase loudspeakers at 400 Hz. The loudspeakers are modeled as simple point sources.

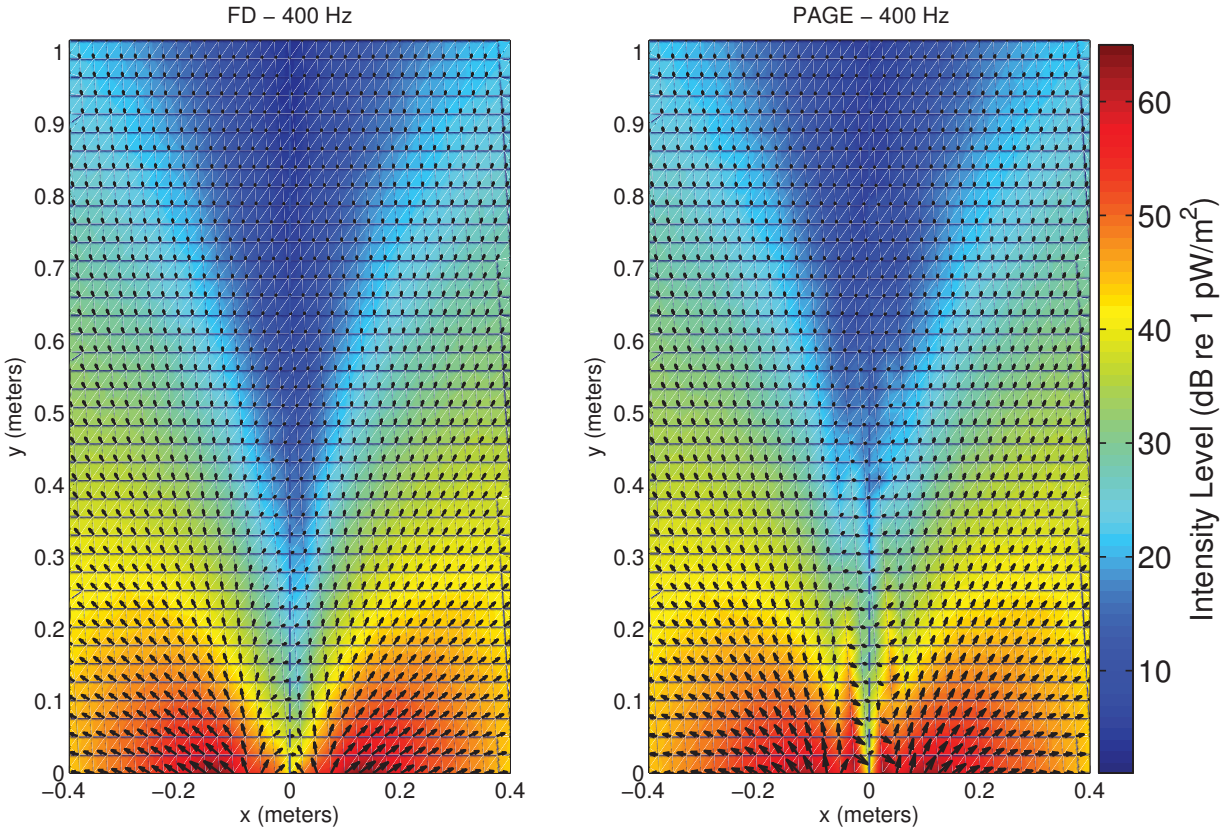

Figure 3.2: The measured acoustic intensity field from two closely spaced, out-of-phase speakers at 400 Hz. Each vector position represents a measurement location. Intensity was processed using both the FD (left) and PAGE (right) methods.

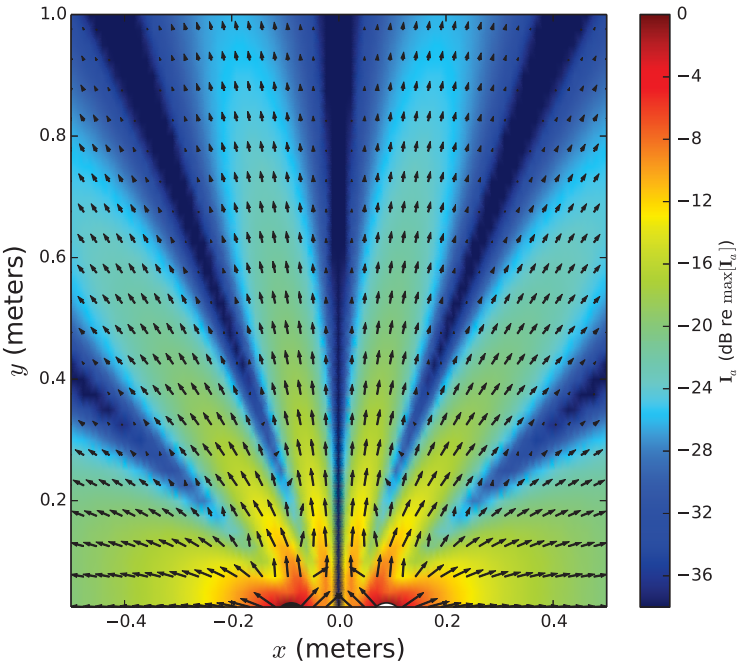

Figure 3.3: The modeled acoustic intensity field from two closely spaced, out-of-phase speakers at 5000 Hz. The loudspeakers are modeled as simple point sources. This is a poor model for these loudspeakers at this frequency since the acoustic wavelength is close to the same size as the diameter of the loudspeakers.

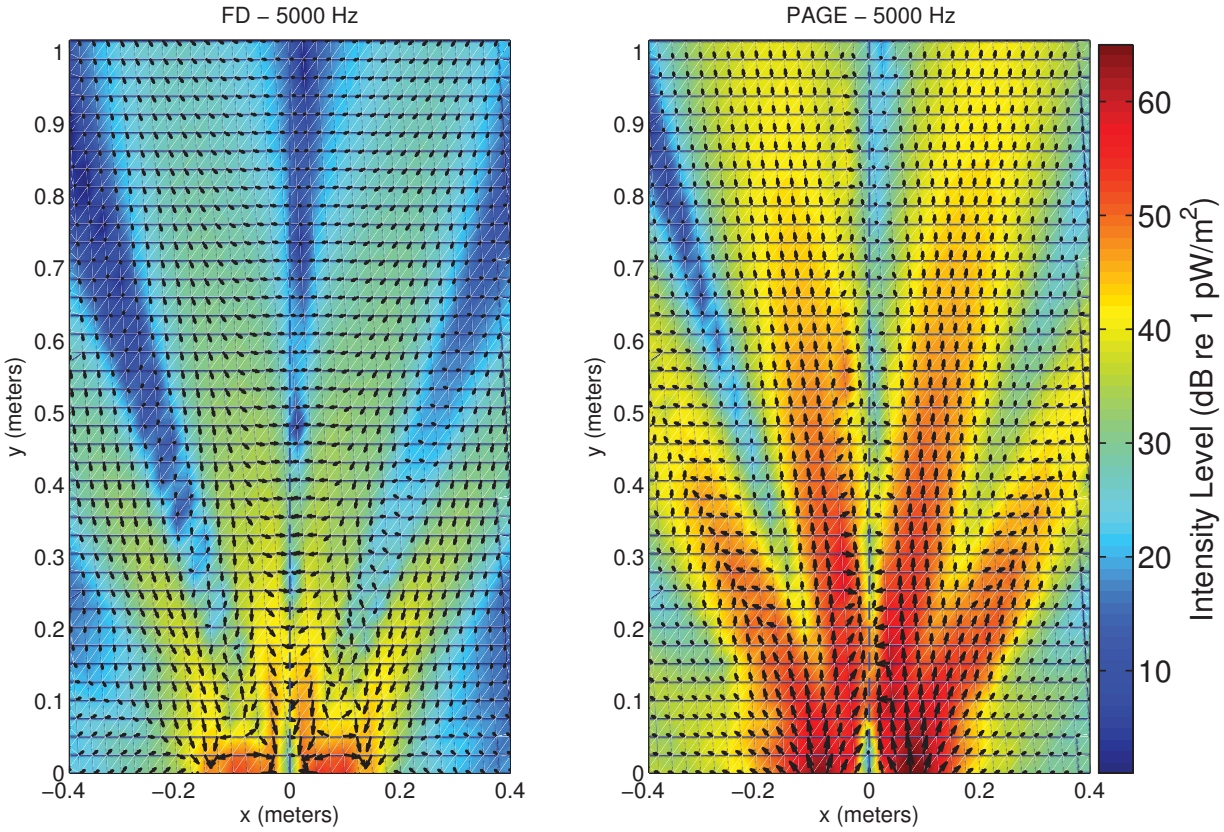

Figure 3.4: The measured acoustic intensity field from two closely spaced, out-of-phase speakers at 5000 Hz. Each vector position represents a measurement location. Intensity was processed using both the FD (left) and PAGE (right) methods.

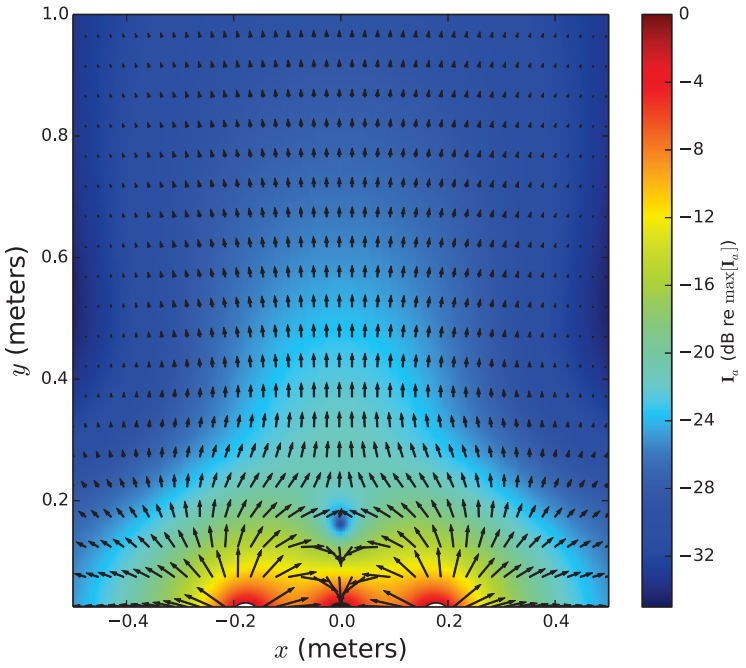

Figure 3.5: The modeled acoustic intensity field from three closely spaced speakers, with the middle speaker out of phase with the outside speakers, at 400 Hz. The loudspeakers are modeled as simple point sources.

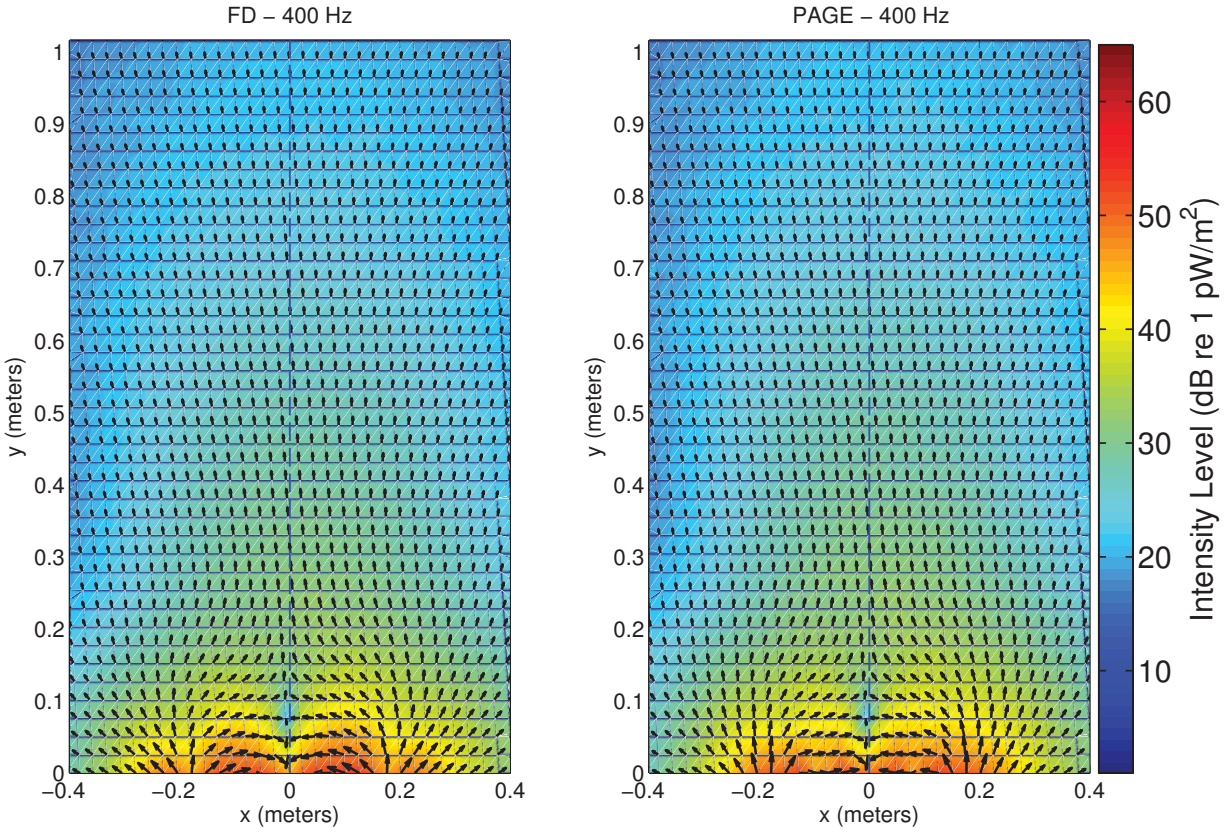

Figure 3.6: The measured acoustic intensity field from three closely spaced speakers, with the middle speaker out of phase with the outside speakers, at 400 Hz. Each vector position represents a measurement location. Intensity was processed using both the FD (left) and PAGE (right) methods.

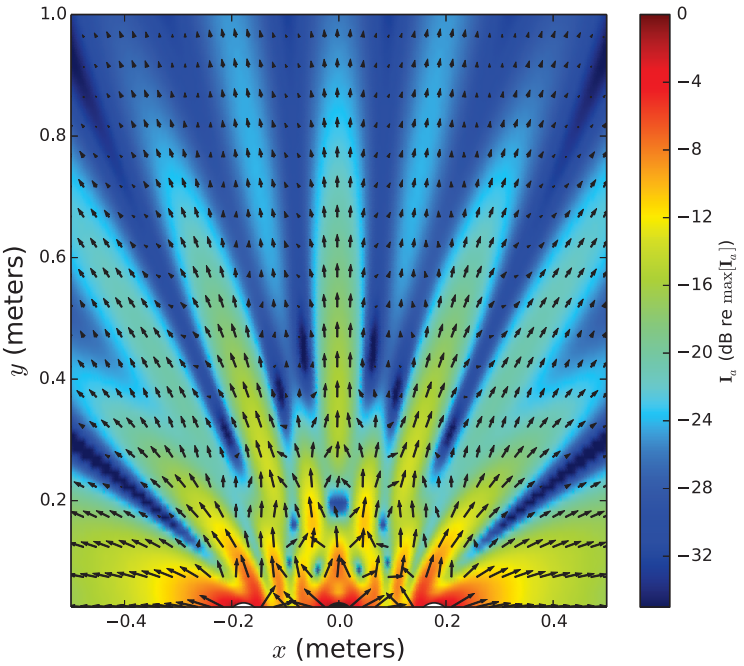

Figure 3.7: The modeled acoustic intensity field from three closely spaced speakers, with the middle speaker out of phase with the outside speakers, at 5000 Hz. The loudspeakers are modeled as simple point sources. This is a poor model for these loudspeakers at this frequency since the acoustic wavelength is close to the same size as the diameter of the loudspeakers.

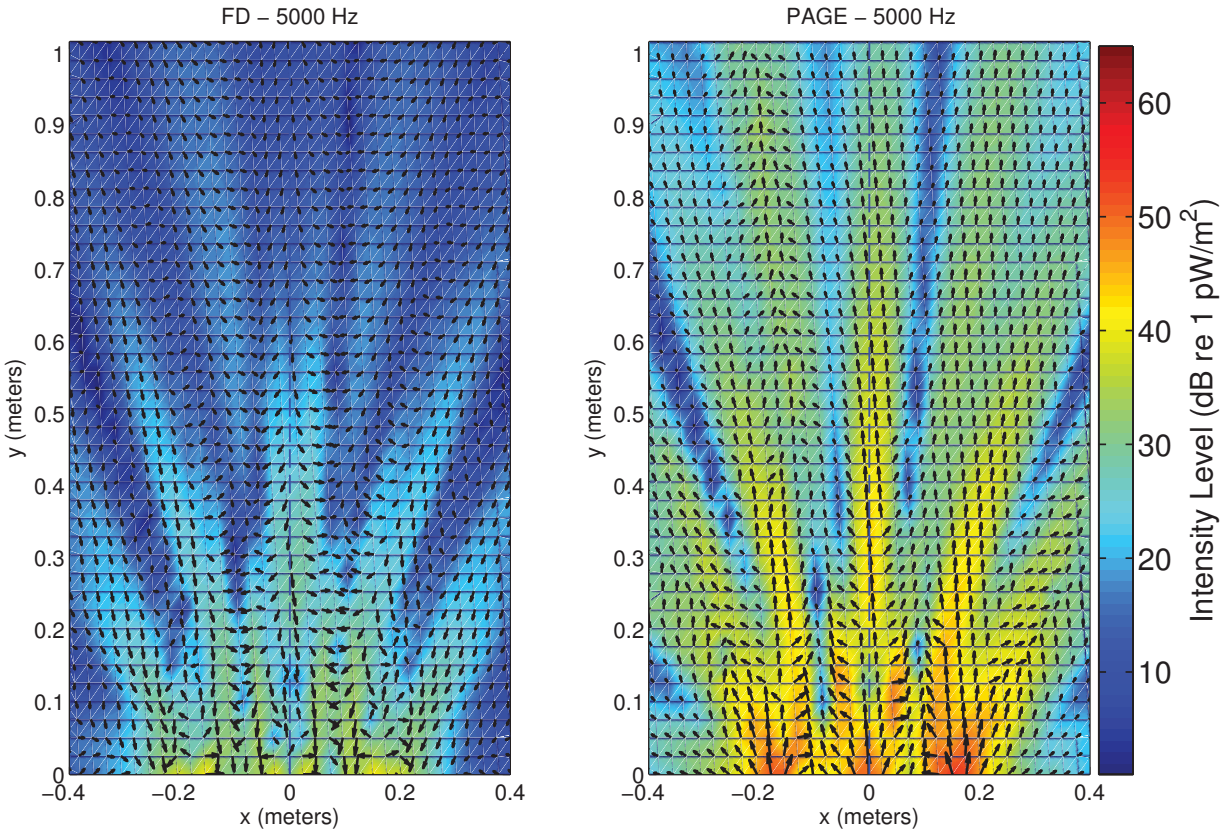

Figure 3.8: The measured acoustic intensity field from three closely spaced speakers, with the middle speaker out of phase with the outside speakers, at 5000 Hz. Each vector position represents a measurement location. Intensity was processed using both the FD (left) and PAGE (right) methods.

Chapter 4

Rocket noise analysis

4.1 GEM-60 measurement setup

The performance of the two acoustic intensity estimation methods was tested in the environment of a full scale rocket on September 6th, 2012. Made possible by ATK, a team of BYU and Blue Ridge Research and Consulting participated in a ground test of a GEM 60 solid rocket motor. This horizontal static test firing occurred in Promontory, Utah at ATK's test facility. The GEM-60 has a 1.09 m (3.59-ft) diameter nozzle with a burn time of approximately 90.8 seconds. Similar measurements of a GEM-60 were taken previously by Gee *et al.*[5,45]

Intensity probes and single microphones along with other transducers were set up in the field near where the rocket would fire. The measurement layout is shown in Fig. 4.1. Sensor location distances are described in terms of nozzle diameters (D) with 1D equaling 1.09 m. Angles are measured with respect to the estimated noise source origin, which is 17D downstream of the nozzle exit. Primarily, the 2D intensity probe discussed in Section 2.3.1 was used along the shear layer of the rocket plume. A 3D tetrahedral probe developed in conjunction with NASA was also used. Both probe designs can be seen in Fig. 4.2.

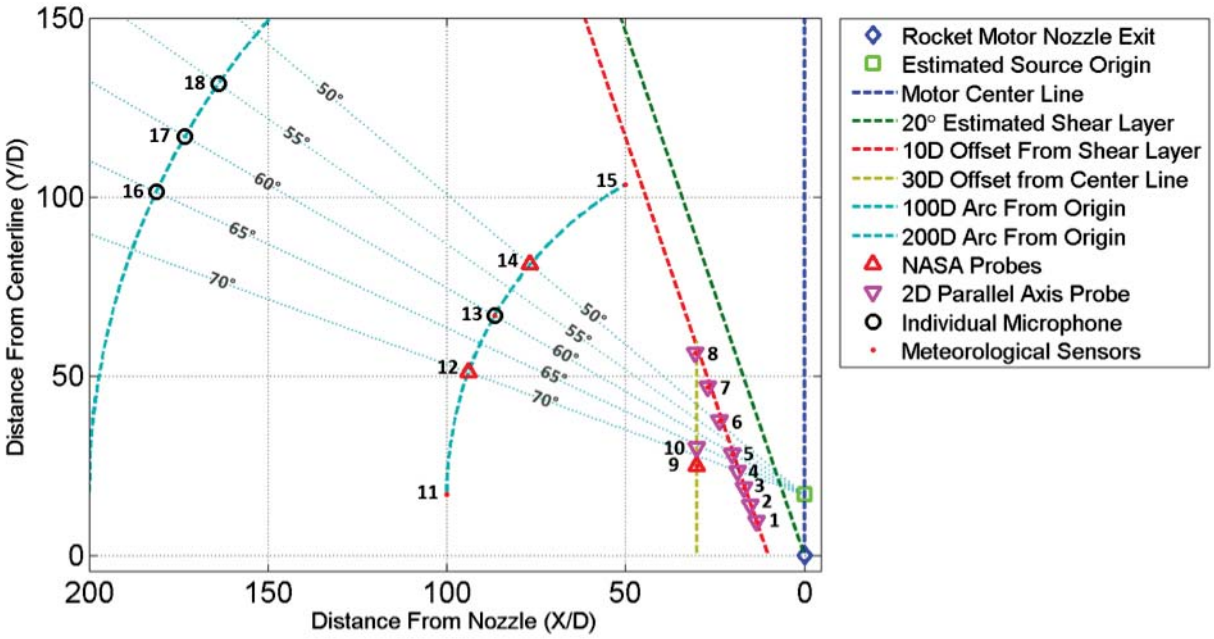

Figure 4.1: GEM-60 measurement layout.

Figure 4.2: 2D intensity probe (left) and NASA spherical 3D intensity probe (right) set for rocket test firing.

The shear-layer array, indicated by the red dotted line in Fig. 4.1, was offset by 10D, 10.95 m, from the rocket plume shear-layer boundary, which was estimated to be at a 20° angle to the centerline. Shear-layer measurement location distances were measured from the nozzle exit plane. Eight 2D probes were deployed at locations 1 through 8, along the shear layer at distances of 10D, 15D, 20D, 25D, 30D, 40D, 50D, 60D from the nozzle exit. These locations were specifically chosen to capture the peak source region.

The parallel array, indicated by locations 9 and 10 along the gold dotted line in Fig. 4.1, was offset by 30D (32.85 m), from the centerline. One 2D probe was located 15D from the nozzle exit indicated by location 9 and one NASA spherical probe was 25D from the nozzle exit at location 10. Two additional arrays were oriented at 100D and 200D circular arcs, indicated in Fig. 4.1 by the teal dotted lines. Along the 100D circular arc, two NASA spherical probes were placed at locations 12 and 14 at 70° and 50° from the motor centerline respectively. Additionally, one individual microphone was placed at location 13 at 60°. Along the 200D arc, three individual microphones were deployed at locations 16, 17 and 18 at angles of 65°, 60°, and 55° respectively.

4.2 GEM-60 intensity vectors

The resulting intensity vectors from the various probes are presented here. Both the finite-difference (FD) and the new phase and amplitude gradient estimation (PAGE) methods of estimating intensity are used. For this test, nine prototypes of the 2D intensity probes were used, as well as three spherical probes developed under a previous program (see Fig. 4.2). To examine the performance of the PAGE and FD methods with the new two-dimensional probes, the intensity magnitudes from two-dimensional and three-dimensional spherical probes are compared in Fig. 4.3 and Fig. 4.4. These plots also include the power-spectral-density (PSD) of the center microphone, with an offset of $10\log_{10}(df)$, where df is the frequency bin-width. For a propagating wave field, the active

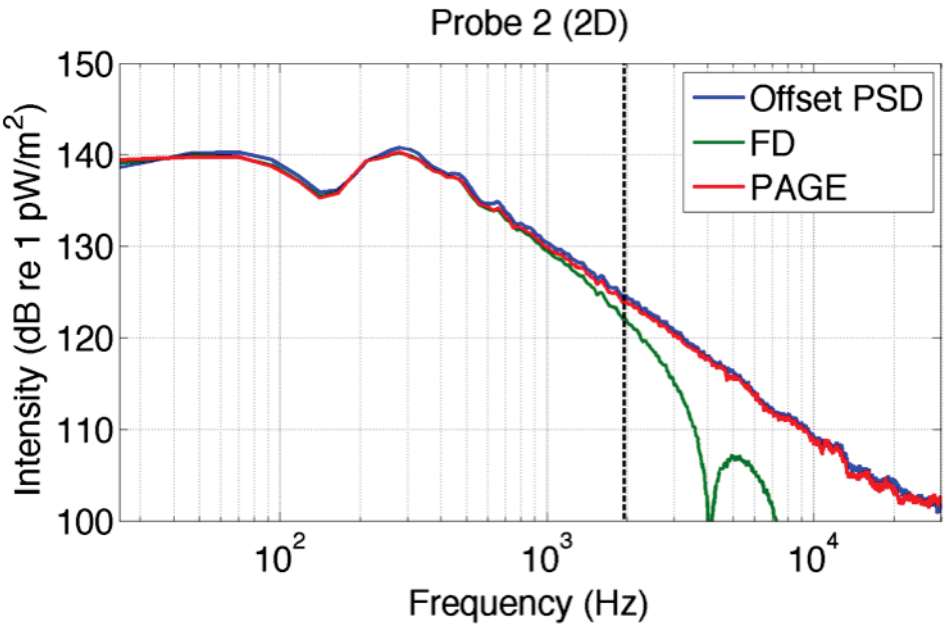

Figure 4.3: Active acoustic intensity magnitude of the GEM-60 using the FD and PAGE methods for the two-dimensional probe (probe 2), compared to the total sound pressure level ("the offset PSD") at the location. For a propagating wave field, the intensity and sound pressure levels should be nearly equal. The vertical dashed line represents the spatial Nyquist limit of the probe. Due to phase unwrapping, the PAGE method is shown to give high-frequency performance that is superior to the FD method.

intensity should have the same magnitude as these offset PSDs, thus they are included for reference. Figure 4.3 shows these quantities for probe 2, which is the second closest probe to the rocket (probe 2 in Fig. 4.1), and Fig. 4.4 is from one of the spherical 3D intensity probes (probe 10). These plots demonstrate the inherent frequency-dependent bias of the FD method, and illustrate how the PAGE method can be used to greatly increase the upper limit for these probes. The PAGE method allows for the phase gradient to be unwrapped, which then yields accurate results beyond the spatial Nyquist frequency. Though in theory, there is no upper frequency limit to the unwrapped PAGE method, in practice we find that it is limited by the noise in the argument of the

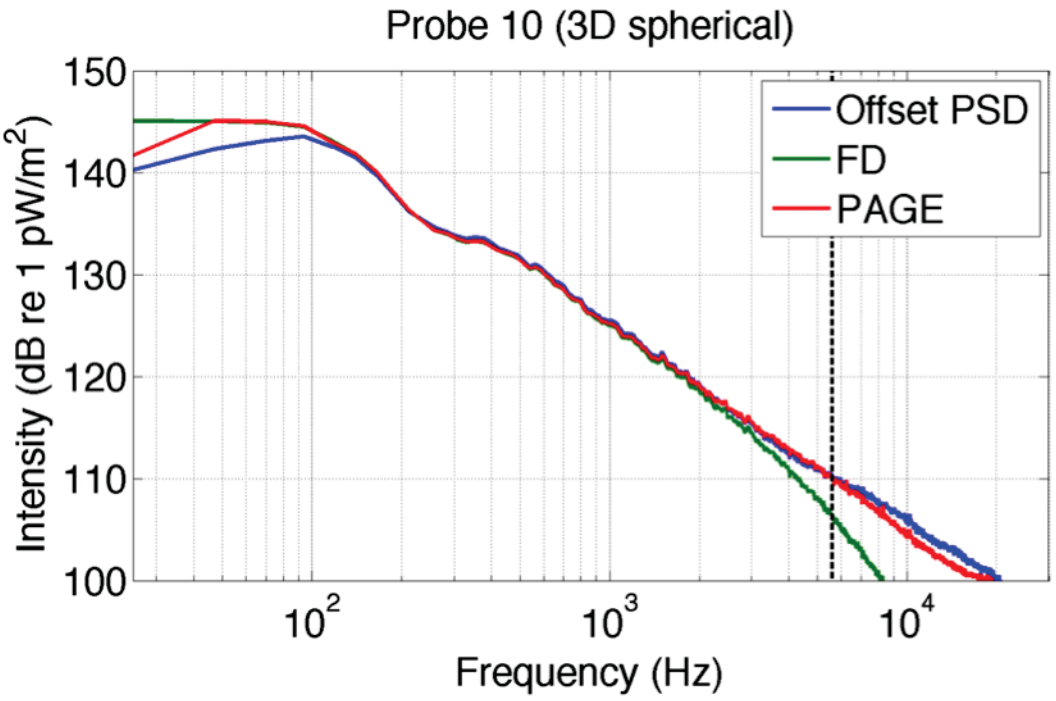

Figure 4.4: The same quantities as Fig. 4.3 are shown here, but for a 3D spherical NASA probe (probe 10). A comparison with Fig. 4.3 shows that the 3D NASA probes do not provide as accurate results at low frequencies due to the smaller spacing of the microphones. As a result of the smaller microphone spacing, the spatial Nyquist frequency is much higher than it is for the 2D probes.

pair-wise transfer functions.

One method to determine the upper frequency limit of the PAGE method intensity estimates is to look at the arguments of the transfer functions between microphones. Figure 4.5 shows these transfer functions for one of the 2D intensity probes, as well as the same functions with unwrapping applied. In this figure, it is clear that the noise in the argument of the transfer function causes the unwrapping to fail at higher frequencies. If more averaging is applied to the same data, the phase function can be accurately unwrapped to higher frequencies, as can be seen in Fig. 4.6. Since the exact frequency where phase unwrapping fails is measurement dependent, it is important to use the argument of the transfer functions to determine the upper frequency limit of a particular

measurement. It is also important to recall that phase unwrapping only works when measuring broadband sources.

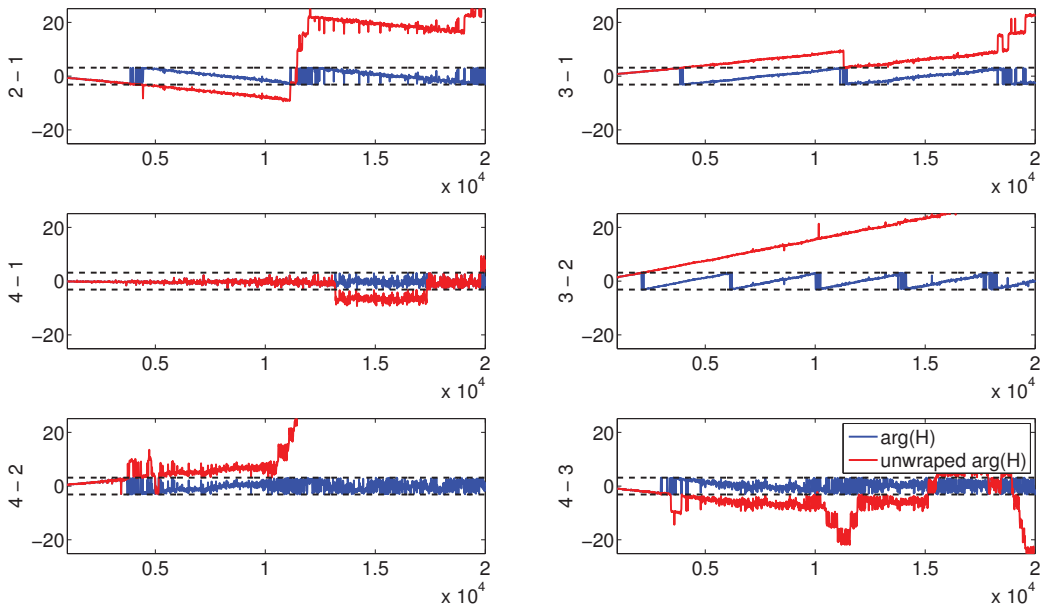

Figure 4.5: The argument of the transfer functions between the four microphones of one of the 2D intensity probes. The black dashed lines represent $\pm\pi$. It can be seen how the noise in the transfer function causes failures in the unwrapping. The averaging here leads to a bin-width of approximately 11 Hz.

With sufficient averaging, the unwrapped PAGE method for the 2D probes breaks down around 10kHz. The spatial Nyquist frequency is around 1950 Hz for the 2D probes and 5600 Hz for the spherical 3D probes. It should be noted that by having a microphone in the center of the probe, finite-sum errors are eliminated in estimating the pressure at the center of the probe. This leads to improved performance of the FD method; namely, it doesn't appear to completely break down until double the Nyquist limit. Overall, large microphone separation distances allows for better low-frequency estimates, while high-frequency estimates are still possible due to the unwrapped

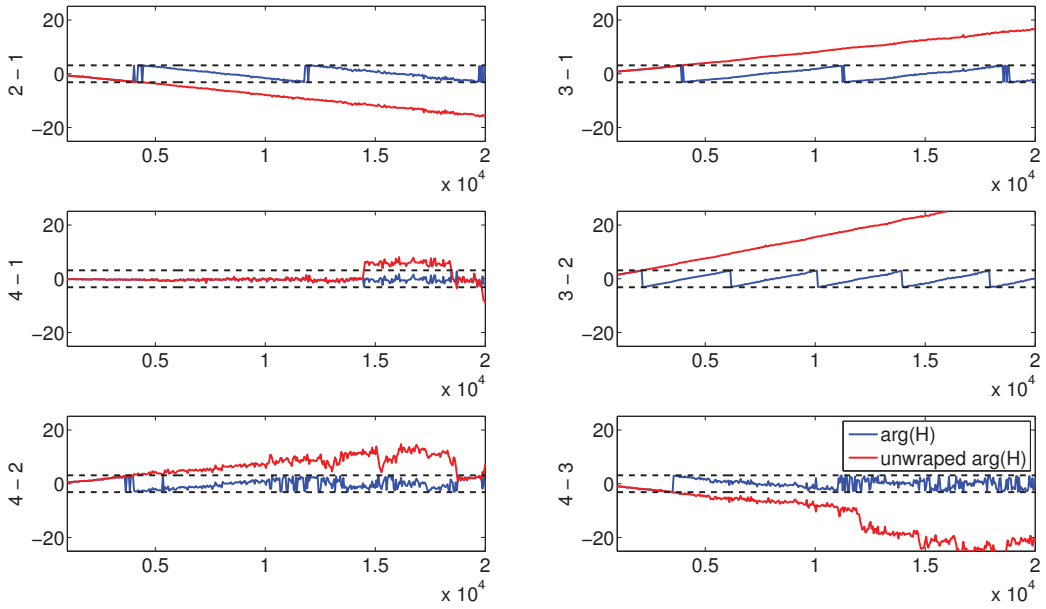

Figure 4.6: The same arguments of transfer functions as Fig. 4.5 are show, but processed with smaller block sizes as to increase the number of averages. This allows the unwrapping to work at higher frequencies but at the cost of larger frequency bins. The plots here have a bin-width of approximately 50 Hz, which is unsuited for investigating lower frequencies.

PAGE methods. Although there are nonlinear propagation effects present in the field, nonlinear acoustic propagation tends to be a cumulative effect. Within the neighborhood of each probe, these cumulative changes due to acoustic nonlinearities are negligible, thus the PAGE method, which is based on linear acoustic theory, is still valid. The effects of local nonlinear effects such as acoustic radiation force have not been considered.

The active intensity magnitudes of all eight probes near the shear-layers are shown in Fig. 4.7. Probe 3 utilized low-sensitivity 3.175 mm (1/8") microphones and as such had a poorer response for low frequencies. The resulting acoustic intensity vectors are shown in Figs. 4.8 and 4.9. It can be seen in these figures that as frequency increases, the apparent source of sound moves closer to

the nozzle and reduces in size. Both methods give comparable results at low frequencies. Overall we see that at higher frequencies the PAGE method outperforms the FD method because it provides accurate intensity vectors beyond the spatial Nyquist limit.

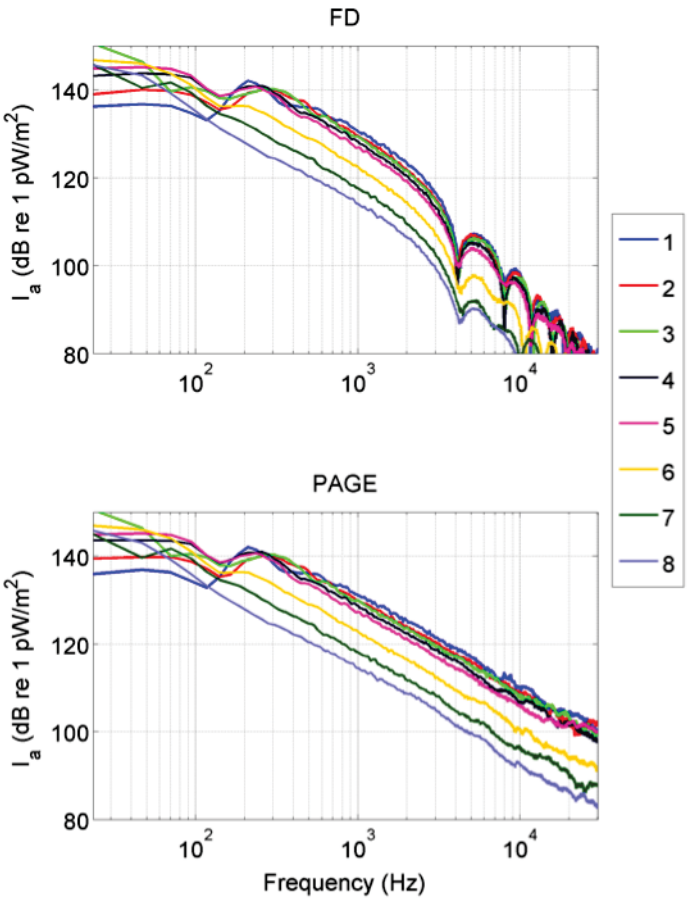

Figure 4.7: The active intensity magnitude estimated from the eight 2D intensity probes parallel to the shear layer. The probes are numbered from closest to farthest from the GEM-60 nozzle (see Fig. 4.1). The estimates calculated through the FD method are accurate up to approximately 1500 Hz, whereas the PAGE estimates appear to be accurate up to approximately 10kHz.

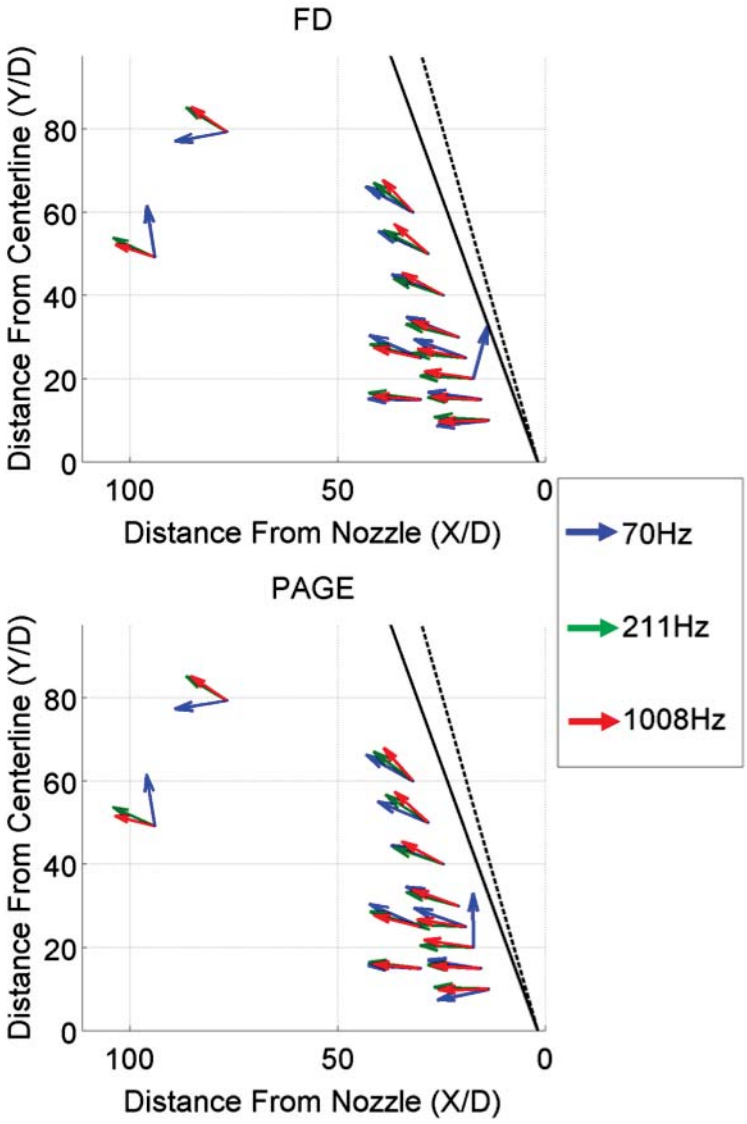

Figure 4.8: The active intensity vectors at select frequencies for all the intensity probes are shown. The vectors have lengths relative to the intensity levels. The black solid and dashed lines represent the 20° and 18° angles from the plume, respectively. At the lowest frequencies, the smaller NASA probes (farthest from source) fail as a result of phase mismatch errors. The 2D probe with 3.175 mm (1/8") microphones (third in the line parallel to the shear layer) also fails at low frequency because of phase mismatch errors.

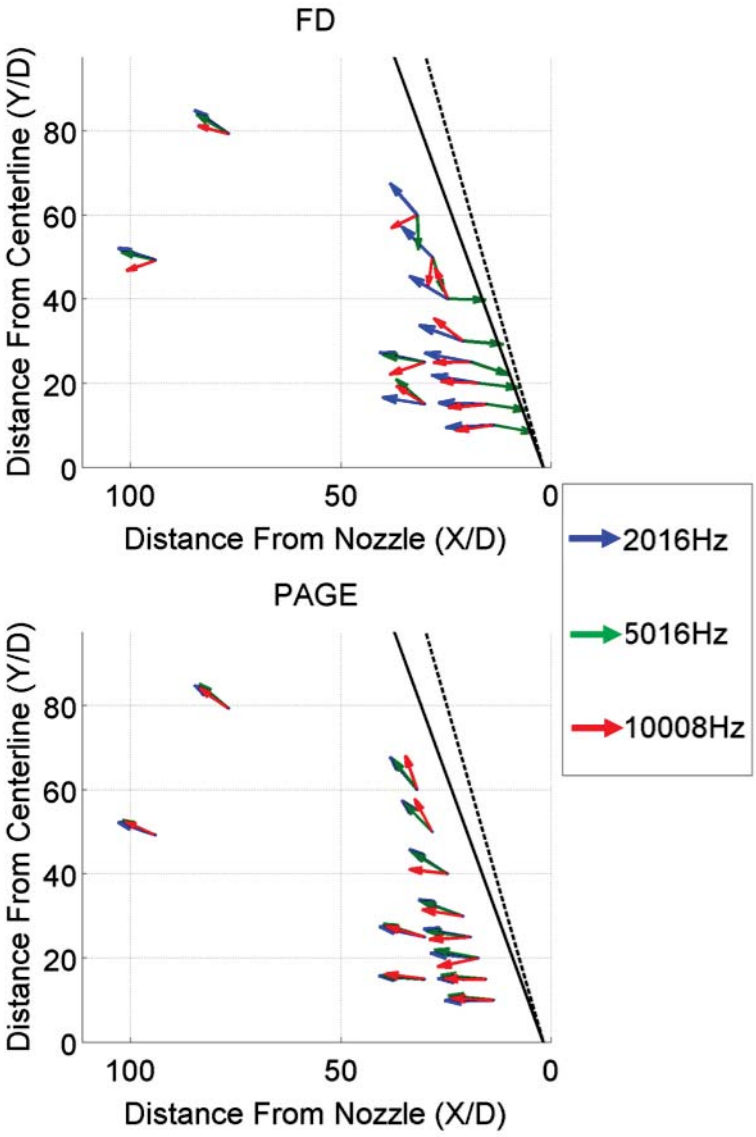

Figure 4.9: The active intensity for three additional frequencies, all above the spatial Nyquist limit of 1950Hz for the 2D probes, are shown. The FD estimates break down while the unwrapped PAGE method allows accurate estimates over this limit. This smaller microphone separation in the NASA probes allows for accurate intensity estimates up to 4kHz. The PAGE method starts to break down around 10kHz.

Chapter 5

Conclusions

Two methods of estimating acoustic intensity have been presented and compared in this work: the traditional finite-difference p-p method and the new phase and amplitude gradient estimator (PAGE) method. Both methods rely on multi-microphone probes, with phase matched microphones. The traditional FD method relies on an estimate of the gradient of the complex pressure. This finite-difference approximation degrades as the microphones become further apart with respect to the wave-length. This causes the estimates produced by the FD method to have a frequency-dependent bias; as frequency increases, the FD method underestimates the intensities. The PAGE method separates the complex pressure into phase and amplitude components, and the gradients of the phase and amplitude are evaluated individually. The phase gradient is found using the argument of pairwise microphone transfer functions. The amplitude gradient is found by simply taking the magnitude of the complex pressures. Estimating the phase and amplitude in lieu of the complex pressure gradient provides for some distinct advantages, which have been the focus of this work. Not only are the resulting intensities more accurate, but the phase component can be unwrapped, allowing for accurate intensity estimates past the spatial Nyquist limit. Because the PAGE and FD methods both rely on multi-microphone probes, the PAGE method can be easily applied to existing p-p intensity probes.

The original motivation behind this work was to improve intensity estimates of rocket noise. As such, a section on the measurement of a recent rocket test firing was included. Several intensity probes were placed in the near field of the rocket, and the intensity from each of these probes was estimated using both methods presented here. As a result of this test, it was found that an offset power spectral density of a single microphone provides a useful indicator for the accuracy of intensity estimates. Using this comparison, it was found that the PAGE method provides for more accurate estimates over a larger frequency range. Using the traditional methods, the large 2D probes presented in Section 2.3.1 should break down at frequencies higher than around 2 kHz, but using the unwrapped PAGE method, accurate estimates were found up to around 10 kHz.

Though this project originally was motivated by rocket noise, the PAGE method can be used in any applications of multi-microphone intensity probes. The PAGE method uses the same hardware as the FD method, thus it can be used to improve the accuracy and frequency range of intensity estimates wherever the FD method is used.

There is still work that can be done to investigate and optimize the PAGE method. For example, the works of Wiederhold *et al.*[35,36,40] could be repeated with the PAGE method. Also, little consideration has been given to different probe geometries. It would be of great interest to investigate the performance of the PAGE method given different probe geometries. It should be noted, however, that the primary advantages of the PAGE method are independent of probe geometry, thus the findings of this thesis should extend to all probe geometries. Another subject which requires future investigation is that of the reactive intensity. The works of Mann *et al.*[37] and Mann and Tichy[2,38] suggest that the reactive component of intensity is needed to fully understand many intensity fields. This work deals primarily with the active intensity, though the means of finding the reactive intensity have been included. Preliminary work shows that for the reactive intensity the advantages of the PAGE method over the FD method are even more distinct, and thus the PAGE method may provide researchers a more accurate and consistent method of measuring reactive in-

tensity fields. A higher order finite-difference method of estimating gradients was also presented, but not elaborated on. The higher order estimates could allow for larger intensity probes given that the field would no longer need to be locally planar. Larger probes would be advantageous because errors caused by phase mismatching would be minimized. This higher order method could also provide more accurate intensity estimates, but further investigation into these methods is left for future work. Another area of future work could be into optimizing phase unwrapping, which would lead to accurate intensity estimates at higher frequencies. Finally, many standards on acoustic intensity rely solely on the FD method, and as such, they could be improved and re-evaluated using the PAGE method.

Appendix A

Higher-order methods

The following section is provided to give an introduction to higher-order estimation methods. There has been little work investigating the advantages of using higher-order estimations with acoustic intensity. This section is provided as a starting point for future work.

Higher-order least-squares approximations can be applied to both the FD and PAGE methods, but require more sensors than the first-order method presented in Section 2.2.1. A brief discussion of the formulation of higher order FD and PAGE methods will be discussed here. To use these higher-order methods, more microphones in each dimension are required. Eq. (2.4) can be extended to a higher term by considering

$$\mathbf{X}\nabla g + \mathbf{X}\nabla(\nabla g)\mathbf{X}^T = \mathbf{\Delta} g + O\left\{\max\left[\left|\frac{\partial^3 g}{\partial x \partial y \partial z}\right| |\mathbf{X}|^3\right]\right\}. \tag{A.1}$$

Equation (A.1) can be simplified into a simpler linear algebra problem if we define a matrix $\mathbf{M}$ as

$$\mathbf{M} = [\mathbf{Q}|\mathbf{X}], \tag{A.2}$$

where $\mathbf{Q}$ is a matrix of quadratic difference terms, and $\mathbf{X}$ is the same matrix of differences from

Eq. (2.4). In two dimensions,

$$\mathbf{Q} = \begin{bmatrix} (x_2-x_1)^2 & (y_2-y_1)^2 & 2(x_2-x_1)(y_2-y_1) \\ (x_3-x_1)^2 & (y_3-y_1)^2 & 2(x_3-x_1)(y_3-y_1) \\ \vdots & \vdots & \vdots \\ (x_N-x_{N-1})^2 & (y_N-y_{N-1})^2 & 2(x_N-x_{N-1})(y_N-y_{N-1}) \end{bmatrix} \tag{A.3}$$

and

$$\mathbf{M} = \begin{bmatrix} (x_2-x_1)^2 & (y_2-y_1)^2 & 2(x_2-x_1)(y_2-y_1) & (x_2-x_1) & (y_2-y_1) \\ (x_3-x_1)^2 & (y_3-y_1)^2 & 2(x_3-x_1)(y_3-y_1) & (x_3-x_1) & (y_3-y_1) \\ \vdots & & \vdots & & \vdots \\ (x_N-x_{N-1})^2 & (y_N-y_{N-1})^2 & 2(x_N-x_{N-1})(y_N-y_{N-1}) & (x_N-x_{N-1}) & (y_N-y_{N-1}) \end{bmatrix}. \tag{A.4}$$

Using this matrix, $\mathbf{M}$, we can rewrite eq Eq. (A.1) as

$$\mathbf{M}\left[\text{vec}(\nabla(\nabla g))|\nabla g\right] = \mathbf{\Delta} g + O\left\{\max\left[\left|\frac{\partial^3 g}{\partial x_i \partial x_j \partial x_k}\right| |\mathbf{X}|^3\right]\right\}, \tag{A.5}$$

where $\text{vec}(\nabla(\nabla g))$ is the vectorized Hessian matrix of g. The second order least-squares estimate of ∇g and $\nabla(\nabla g)$ can now be written as

$$[\text{vec}(\nabla(\nabla g))|\nabla g] \approx (\mathbf{M}^T\mathbf{M})^{-1}\mathbf{M}^T\mathbf{\Delta} g. \tag{A.6}$$

This higher order method gives more accurate gradients of the quantity g. For $\mathbf{M}^T\mathbf{M}$ to be invertible, there must be at least 3 sensors in each direction. For the 2D case, at least 5 sensor locations would be required, which would lead to $\mathbf{M}$ being a 10x5 matrix.

If we apply this higher-order method to both the finite-difference p-p method as well as the new PAGE method, we get more accurate gradients and, as a result, better estimates. This method is particularly beneficial in fields with large reactive components. It should again be noted that this method requires more sensors than the traditional finite-difference method.

Bibliography

[1] K. M. Eldred, "Acoustic loads generated by the propulsion system," Technical Report No. NASA SP-8072 (1971) .

[2] J. A. Mann III and J. Tichy, "Acoustic intensity analysis: Distinguishing energy propagation and wave-front propagation," The Journal of the Acoustical Society of America **90,** 20–25 (1991).

[3] "Primer: Sound Intensity," Brüel & Kjær application notes (1993).

[4] M. M. James and K. L. Gee, "Advanced acoustic measurement system for rocket noise source characterization," In *Proc. Internoise*, pp. 7602–7614 (2012).

[5] K. L. Gee, J. H. Giraud, J. D. Blotter, and S. D. Sommerfeldt, "Energy-based acoustical measurements of rocket noise," AIAA paper 3165 (2009).

[6] K. L. Gee, J. H. Giraud, J. D. Blotter, and S. D. Sommerfeldt, "Near-field vector intensity measurements of a small solid rocket motor," The Journal of the Acoustical Society of America **128,** EL69–EL74 (2010).

[7] J. H. Giraud, K. L. Gee, and J. E. Ellsworth, "Acoustic temperature measurement in a rocket noise field," The Journal of the Acoustical Society of America **127,** EL179–EL184 (2010).

[8] M. R. Bai, S.-W. Juan, and C.-C. Chen, "Particle velocity estimation based on a two-microphone array and Kalman filter," The Journal of the Acoustical Society of America **133,** 1425–1432 (2013).

[9] G. W. Elko, "An acoustic vector-field probe with calculable obstacle bias," In *Proc. Noise-Con*, **91,** 525–532 (1991).

[10] D. C. Thomas, Master's thesis, Brigham Young University, Provo, Utah, 2008.

[11] "Electroacoustics – Instruments for the measurement of sound intensity – Measurement with pairs of pressure sensing microphones," IEC 1043, International Electrotechnical Commissi, Geneva, Switzerland (1993) .

[12] "Instruments for the Measurement of Sound Intensity," ANSI/ASA S1.9, American National Standards Institute, New York, New York (1996) .

[13] "Acoustics - Noise Emmited by Machinery and Equipment - Engineering Method for the Determination of Emission Sound Pressure Levels in situ at the Work Station and at Other Specified Positions Using Sound Intensity," ISO 11205, International Organization for Standardization, Geneva, Switzerland (2003) .

[14] "Acoustics - Measurement of Sound Insulation in Buildings and of Building Elements Using Sound Intensity - Part 1: Laboratory Measurements," ISO 15186-1, International Organization for Standardization, Geneva, Switzerland (2000) .

[15] "Acoustics - Measurement of Sound Insulation in Buildings and of Building Elements Using Sound Intensity - Part 1: Field Measurements," ISO 15186-1, International Organization for Standardization, Geneva, Switzerland (2003) .

[16] "Acoustics - Determination of sound power levels of noise sources using sound intensity - Part 1: Measurement at Discrete Points," ISO 9614-1, International Organization for Standardization, Geneva, Switzerland (1993) .

[17] "Acoustics - Determination of sound power levels of noise sources using sound intensity - Part 2: Measurement by Scanning," ISO 9614-2, International Organization for Standardization, Geneva, Switzerland (1996) .

[18] "Acoustics - Determination of sound power levels of noise sources using sound intensity - Part 3: Precision Method for Measurement by Scanning," ISO 9614-3, International Organization for Standardization, Geneva, Switzerland (2002) .

[19] F. Fahy, in *Sound Intensity* (E. & F.N. Spon, London, 2002), pp. 1–295.

[20] F. Jacobsen, "Sound intensity," in *Springer Handbook of Acoustics*, T. D. Rossing, ed., (Springer, New York, New York, 2007), pp. 961–1017.

[21] F. Jacobsen, "Sound intensity measurements," in *Handbook of Noise and Vibration Control*, M. J. Crocker, ed., (John Wiley & Sons, Hoboken, N.J., 2007), pp. 534–548.

[22] M. J. Crocker, "Measurement of sound intensity," in *Handbook of Acoustical Measurements and Noise Control*, C. M. Harris, ed., (McGraw-Hill, New York, New York, 1991), pp. 14.1–14.17.

[23] U. S. Shirahatti and M. J. Crocker, "Two-microphone finite difference approximation errors in the interference fields of point dipole sources," The Journal of the Acoustical Society of America **92,** 258 (1992).

[24] R. Raangs, W. F. Druyvesteyn, and H. E. De Bree, "A low-cost intensity probe," Journal of the Audio Engineering Society **51,** 344–357 (2003).

[25] T. A. Stout, K. L. Gee, T. B. Neilsen, A. T. Wall, D. W. Krueger, and M. M. James, "Preliminary analysis of acoustic intensity in a military jet noise field," Proceedings of Meetings on Acoustics 19 (2013).

[26] J. H. Giraud, K. L. Gee, S. D. Sommerfeldt, R. T. Taylor, and J. D. Blotter, "Low-frequency calibration of a multidimensional acoustic intensity probe for application to rocket noise," Proceedings of Meetings on Acoustics 14 (2013).

[27] F. Jacobsen and H.-E. de Bree, "A comparison of two different sound intensity measurement principles," The Journal of the Acoustical Society of America **118,** 1510 (2005).

[28] F. Jacobsen, V. Cutanda, and P. M. Juhl, "A numerical and experimental investigation of the performance of sound intensity probes at high frequencies," The Journal of the Acoustical Society of America **103,** 953 (1998).

[29] G. W. Elko, Ph.D. thesis, The Pennsyvania State University, 1984.

[30] J. W. Parkins, S. D. Sommerfeldt, and J. Tichy, "Error analysis of a practical energy density sensor," The Journal of the Acoustical Society of America **108,** 211 (2000).

[31] R. Hickling and A. W. Brown, "Determining the direction to a sound source in air using vector sound-intensity probes," The Journal of the Acoustical Society of America **129,** 219–224 (2011).

[32] G. Rasmussen, "Measurement of vector fields," In *Proceedings of the 2nd International Congress on Acoustic Intensity*, pp. 53–58 (1985).

[33] B. S. Cazzolato and C. H. Hansen, "Errors arising from three-dimensional energy density sensing in one-dimensional sound fields," Journal of sound and vibration **236,** 375–400 (2000).

[34] B. S. Cazzolato and C. H. Hansen, "Errors in the measurement of acoustic energy density in one-dimensional sound fields," Journal of sound and vibration **236,** 801–831 (2000).

[35] C. P. Wiederhold, Master's thesis, Brigham Young University, Provo, Utah, 2011.

[36] C. P. Wiederhold, K. L. Gee, J. D. Blotter, S. D. Sommerfeldt, and J. H. Giraud, "Comparison of multimicrophone probe design and processing methods in measuring acoustic intensity," The Journal of the Acoustical Society of America **135,** 2797–2807 (2014).

[37] J. A. Mann III, J. Tichy, and A. J. Romano, "Instantaneous and time-averaged energy transfer in acoustic fields," The Journal of the Acoustical Society of America **82,** 17–30 (1987).

[38] J. A. Mann III and J. Tichy, "Near-field identification of vibration sources, resonant cavities, and diffraction using acoustic intensity measurements," The Journal of the Acoustical Society of America **90,** 720–729 (1991).

[39] J.-C. Pascal and J.-F. Li, "A systematic method to obtain 3D finite-difference formulations for acoustic intensity and other energy quantities," Journal of Sound and Vibration **310,** 1093 – 1111 (2008).

[40] C. P. Wiederhold, K. L. Gee, J. D. Blotter, and S. D. Sommerfeldt, "Comparison of methods for processing acoustic intensity from orthogonal multimicrophone probes," The Journal of the Acoustical Society of America **131,** 2841 (2012).

[41] K. H. Miah and E. L. Hixon, "Design and performance evaluation of a broadband three dimensional acoustic intensity measuring system," The Journal of the Acoustical Society of America **127,** 2338–2346 (2010).

[42] H. Suzuki, S. Oguro, M. Anzai, and T. Ono, "Performance evaluation of a three dimensional intensity probe.," Journal of the Acoustical Society of Japan (E) **16,** 233–238 (1995).

[43] C. A. Szuberla and J. V. Olson, "Uncertainties associated with parameter estimation in atmospheric infrasound arrays," The Journal of the Acoustical Society of America **115,** 253–258 (2003).

[44] S. T. Smith, "Covariance, subspace, and intrinsic Cramér-Rao bounds," IEEE Trans. Signal Processing **53,** 1610–1630 (2005).

[45] J. H. Giraud, Master's thesis, Brigham Young University, Provo, Utah, 2012.